

WHAT CAN WE LEARN ABOUT THE KINEMATICS OF BRIGHT EXTRAGALACTIC PLANETARY NEBULAE?¹

M. G. Richer,² S.-H. Báez,³ J. A. López,² H. Riesgo,² and M. T. García-Díaz²

Received 2009 May 3; accepted 2009 August 14

RESUMEN

Presentamos espectroscopía de alta resolución en las líneas de [O III] λ 5007 y H α de nebulosas planetarias (NPs) brillantes en el bulbo de nuestra Vía Láctea así como las galaxias enanas M32, Fornax, Sagittarius y NGC 6822, obtenida en el Observatorio Astronómico Nacional en la Sierra San Pedro Mártir con el espectrógrafo Manchester echelle. Utilizamos las observaciones profundas de las NPs galácticas para determinar la información cinemática confiable que puede obtenerse mediante las observaciones mucho menos profundas de las NPs extragalácticas observadas en la línea de [O III] λ 5007. Encontramos que la anchura intrínseca de las líneas en [O III] λ 5007 y H α son similares, que la anchura no depende de la relación señal a ruido (dentro del intervalo cubierto por la muestra), y que las desviaciones respecto a una forma gaussiana son pequeñas. Concluimos que la anchura de la línea de [O III] λ 5007 en NPs extragalácticas refleja de manera fiel la cinemática de la mayoría de la masa de la cáscara ionizada.

ABSTRACT

We present high resolution spectroscopy in the [O III] λ 5007 and H α lines of bright planetary nebulae in the Milky Way bulge and the dwarf galaxies M32, Fornax, Sagittarius, and NGC 6822 obtained at the Observatorio Astronómico Nacional in the Sierra San Pedro Mártir using the Manchester Echelle Spectrograph. We use the high signal-to-noise (S/N) observations of Milky Way bulge planetary nebulae to explore what kinematic information can be determined reliably when observing extragalactic planetary nebulae in the [O III] λ 5007 line at modest S/N. We find that the intrinsic line widths measured in [O III] λ 5007 and H α are very similar. Over the range of S/N available in this sample, the line width we measure is independent of the S/N. Finally, deviations from a Gaussian line shape are small. Thus, the line width of the [O III] λ 5007 line in bright extragalactic planetary nebulae should reflect the kinematics of most of the mass in the ionized nebular shell.

Key Words: Galaxy: bulge — ISM: kinematics and dynamics — planetary nebulae: general — stars: evolution

1. INTRODUCTION

Past and present efforts to study the kinematics of galactic and extragalactic planetary nebulae have produced large and rapidly growing databases of these observations (e.g., Dopita et al. 1985, 1988; Gesicki & Zijlstra 2000; Medina et al. 2006; Arnaboldi et al. 2008; López et al. 2009, in prepara-

tion; Richer et al. 2009, in preparation). However, observations of galactic and extragalactic planetary nebulae often differ in fundamental ways. Typically, galactic planetary nebulae are resolved by the (usually ground-based) spectrograph slit, whereas extragalactic planetary nebulae usually are not. Furthermore, the kinematics are often measured from different emission lines in galactic (e.g., H α or [N II] λ 6584) and extragalactic (e.g., [O III] λ 5007) planetary nebulae. It is not necessarily obvious, therefore, how to compare the kinematics of galactic and extragalactic planetary nebulae, so experiments that help us understand exactly what information is available when

¹The observations reported herein were obtained at the Observatorio Astronómico Nacional in the Sierra San Pedro Mártir (OAN-SPM), B. C., Mexico.

²OAN, Instituto de Astronomía, Universidad Nacional Autónoma de México, Mexico.

³Facultad de Física e Inteligencia Artificial, Universidad Veracruzana, Mexico.

studying the kinematics of extragalactic planetary nebulae are worthwhile.

The existing literature (Dopita et al. 1985, 1988; Zijlstra et al. 2006; Arnaboldi et al. 2008) as well as our own observations (Richer et al. 2009, in preparation) indicate that the line profiles of extragalactic planetary nebulae are usually approximately Gaussian. In almost all cases, these are spatially unresolved observations. Obviously, the kinematic information available from such line profiles will be limited, even at high signal-to-noise (S/N; e.g., Morisset & Stasińska 2008). A variety of studies exist of the effect of limited spatial resolution on kinematic studies using models as test cases (e.g., Gesicki & Zijlstra 2000; Rozas et al. 2007). The experiments of Morisset & Stasińska (2008) demonstrate how different structures are visible in different emission lines and with different slit sizes or positions. From their results, it is clear that smaller, precisely positioned slits allow the study of finer detail involving components of lower mass, a fact long exploited in observational studies (e.g., see Sabbadin et al. 2008; García-Díaz et al. 2008; Santander-García et al. 2008, for recent examples). None of these kinematic studies include the hydrodynamic effects that will occur in real nebulae, as do the models of Villavier, Manchado, & García-Segura (2002) and Perinotto et al. (2004). The most detailed hydrodynamical study is perhaps that of Schönberner, Jacob, & Steffen (2005) who emphasize the important differences between the motions of matter and shock fronts (see Corradi et al. 2007 for an application to observations).

While instructive, these studies require particular assumptions for the construction of the models and it is not always clear how closely they match real planetary nebulae. Furthermore, there is often a focus on extracting fine details rather than studying the bulk motion of the majority of the mass. Considering the aforementioned experiments, studies of the line profiles of extragalactic planetary nebulae (Dopita et al. 1985, 1988; Zijlstra et al. 2006; Arnaboldi et al. 2008) will most profitably focus upon the bulk motion of matter in their ionized shells, since the lack of spatial resolution and limited signal-to-noise (S/N) will render small-scale features difficult to discern, even if they have distinctive kinematics.

At the modest S/N that observations achieve, two issues arise: the recovery of the available information and the interpretation of this information in terms of the kinematics. Here, we focus on the former, investigating the empirical description of the line profile, rather than on the interpretation of the

kinematic information that may be derived from it. We aim to determine whether the information available may be recovered reliably and whether this information pertains to the entire nebular shell or to some small fraction of it. Three aspects are most important. First, extragalactic planetary nebulae will usually be studied in the [O III] λ 5007 line, since it is the brightest line in the optical spectrum (and often in the entire spectrum). How well does this line probe the kinematics of the entire ionized mass? Second, the faintness of the [O III] λ 5007 emission in extragalactic planetary nebulae means that the S/N will be modest. How does the limited S/N affect the derived kinematics (e.g., the line width)? Third, the modest S/N will often limit the information available to model the line profile to a simple function, such as a Gaussian (e.g., Dopita et al. 1985, 1988; Arnaboldi et al. 2008). To what extent does such a simple empirical description adequately reflect the kinematics of the ionized mass?

Here, we perform an experiment using observations of bright planetary nebulae in the Milky Way bulge (henceforth, Bulge). Our intent is to use these observations to infer the limitations inherent to kinematic observations of extragalactic planetary nebulae. We have chosen our sample of Bulge planetary nebulae in a way that we hope simulates populations of bright extragalactic planetary nebulae in environments without star formation (§ 2). We obtain high resolution spectra in both the H α and [O III] λ 5007 lines. We analyse the resulting data in the same way we would analyse those for extragalactic planetary nebulae (§ 3). In particular, we use our high S/N spectra to simulate extragalactic observations, normalizing the [O III] λ 5007 spectra to the total fluxes typical of extragalactic observations and adding noise, analyse these synthetic spectra, and compare the results to the original observations. We then consider the three questions posed above (§ 4). We find that the [O III] λ 5007 line widths are similar to the H α line widths, that the observed [O III] λ 5007 line widths are not a function of S/N, at least for the S/N levels typical of spectra of extragalactic planetary nebulae, and that the line width is an adequate description of most of the emission observed, and so representative of the great majority of the ionized mass (§ 5). Hence, we conclude that the kinematics of the ionized shells of extragalactic planetary nebulae may be studied reliably using the [O III] λ 5007 line (§ 6).

2. OBSERVATIONS AND REDUCTIONS

Our sample of planetary nebulae in the Milky Way bulge is given in Tables 1–2 and was selected to

TABLE 1
DEEP AND SHALLOW [O III] λ 5007 SPECTRA

Object	PN G	Run	[O III] λ 5007 deep spectrum				[O III] λ 5007 shallow spectrum	
			Flux (10^3 ADU)	FWHM (\AA)	$\Delta V_{0.5}$ (km/s)	Residual	Flux (10^3 ADU)	FWHM (\AA)
Bl 3-13	000.9-02.0	2006 Jun	268.8 \pm 3.1	0.6063 \pm 0.0079	16.93 \pm 0.24	0.088	19.75 \pm 0.34	0.646 \pm 0.012
Cn 1-5	002.2-09.4	2004 Jun	4809.6 \pm 155.1	1.251 \pm 0.041	36.9 \pm 1.2	0.203	322.43 \pm 10.15	1.272 \pm 0.041
Cn 2-1	356.2-04.4	2004 Jun	2084.6 \pm 20.3	0.6826 \pm 0.0074	19.36 \pm 0.22	0.106	390.78 \pm 3.67	0.6806 \pm 0.0071
H 1-1	343.4+11.9	2004 Jun	778.9 \pm 26.1	1.238 \pm 0.043	36.5 \pm 1.3	0.227	159.75 \pm 5.15	1.236 \pm 0.042
H 1-11	002.6+08.2	2006 Jun	906.3 \pm 14.1	0.625 \pm 0.011	17.53 \pm 0.32	0.140	46.09 \pm 0.84	0.642 \pm 0.013
H 1-14	001.7+05.7	2005 Jul	484.3 \pm 24.6	1.3134 \pm 0.068	38.8 \pm 2.0	0.352	19.19 \pm 1.09	1.284 \pm 0.075
H 1-16	000.1+04.3	2005 May	540.5 \pm 8.1	0.743 \pm 0.012	21.25 \pm 0.36	0.112	17.97 \pm 0.41	0.761 \pm 0.019
H 1-17	358.3+03.0	2005 Jul	221.2 \pm 2.4	0.6150 \pm 0.0072	17.20 \pm 0.22	0.094	1.97 \pm 0.17	0.766 \pm 0.072
H 1-18	357.6+02.6	2004 Jun	267.5 \pm 1.8	0.5062 \pm 0.0039	13.66 \pm 0.12	0.075	4.60 \pm 0.17	0.56 \pm 0.023
H 1-20	358.9+03.2	2003 Jun	361.7 \pm 2.0	0.6905 \pm 0.0042	19.53 \pm 0.13	0.048	38.95 \pm 0.54	0.691 \pm 0.011
H 1-23	357.6+01.7	2005 May	264.2 \pm 5.3	0.754 \pm 0.016	21.62 \pm 0.49	0.164	23.46 \pm 0.49	0.778 \pm 0.018
H 1-27	005.0+04.4	2003 Jun	564.1 \pm 5.5	0.7004 \pm 0.0075	19.94 \pm 0.22	0.095	60.02 \pm 0.64	0.7093 \pm 0.0083
H 1-30	352.0-04.6	2006 Jun	334.5 \pm 2.6	0.6000 \pm 0.0052	16.73 \pm 0.16	0.091	18.36 \pm 0.27	0.610 \pm 0.010
H 1-31	355.1-02.9	2005 May	1395.9 \pm 7.3	0.6646 \pm 0.0038	18.79 \pm 0.11	0.056	77.48 \pm 0.51	0.6691 \pm 0.0048
H 1-32	355.6-02.7	2005 May	1202.3 \pm 8.1	0.4385 \pm 0.0033	11.37 \pm 0.10	0.082	114.59 \pm 0.79	0.4451 \pm 0.0035
H 1-33	355.7-03.0	2004 Jun	558.4 \pm 2.1	0.5218 \pm 0.0022	14.17 \pm 0.07	0.044	57.63 \pm 0.34	0.5187 \pm 0.0035
H 1-40	359.7-02.6	2005 May	376.0 \pm 7.5	0.643 \pm 0.014	18.09 \pm 0.42	0.187	27.95 \pm 0.60	0.640 \pm 0.015
H 1-41	356.7-04.8	2006 Jun	1906.4 \pm 30.2	0.832 \pm 0.014	24.05 \pm 0.43	0.117	140.35 \pm 2.47	0.834 \pm 0.016
H 1-42	357.2-04.5	2006 Jul	128.8 \pm 1.7	0.5362 \pm 0.0080	14.65 \pm 0.24	0.139	285.75 \pm 3.66	0.537 \pm 0.0075
H 1-45	002.0-02.0	2005 Jul	249.8 \pm 2.6	1.016 \pm 0.011	29.70 \pm 0.34	0.082	5.93 \pm 0.26	1.159 \pm 0.054
H 1-50	358.7-05.2	2004 Jun	422.0 \pm 1.9	0.7291 \pm 0.0038	20.82 \pm 0.11	0.043		
H 1-54	002.1-04.2	2007 Aug	981.5 \pm 4.6	0.5304 \pm 0.0028	14.50 \pm 0.08	0.052	89.04 \pm 0.49	0.5394 \pm 0.0033
H 1-56	001.7-04.6	2007 Aug	941.9 \pm 7.1	0.5650 \pm 0.0048	15.67 \pm 0.14	0.070	60.84 \pm 0.46	0.5637 \pm 0.0047
H 1-59	003.8-04.3	2005 May	387.4 \pm 11.1	1.115 \pm 0.033	32.76 \pm 0.99	0.214	10.63 \pm 0.36	1.237 \pm 0.044
H 1-60	004.2-04.3	2005 May	775.7 \pm 13.5	0.672 \pm 0.013	19.04 \pm 0.38	0.144	38.60 \pm 0.68	0.681 \pm 0.013
H 1-67	009.8-04.6	2005 Jul	1324.2		0.00 \pm 0.00	0.000	35.02 \pm 1.20	0.506 \pm 0.019
H 2-10	358.2+03.5	2004 Jun	210.7 \pm 0.9	0.7907 \pm 0.0038	22.75 \pm 0.11	0.027	17.33 \pm 0.29	0.851 \pm 0.016
H 2-11	000.7+04.7	2005 Jul	22.7 \pm 0.2	0.4684 \pm 0.0055	12.39 \pm 0.16	0.000	3.36 \pm 0.16	0.564 \pm 0.030
H 2-18	006.3+04.4	2004 Jun	496.7 \pm 12.1	1.118 \pm 0.028	32.84 \pm 0.85	0.174	17.56 \pm 0.61	1.096 \pm 0.040
Hb 8	003.8-17.1	2004 Jun	1207.7 \pm 6.4	0.6465 \pm 0.0037	18.21 \pm 0.11	0.052	271.81 \pm 1.22	0.6433 \pm 0.0033
He 2-250	000.7+03.2	2003 Jun	63.8 \pm 1.0	0.797 \pm 0.013	22.98 \pm 0.40	0.056	8.00 \pm 0.51	0.865 \pm 0.059
Hf 2-1	355.4-04.0	2005 May	1115.8 \pm 58.9	1.285 \pm 0.069	37.9 \pm 2.0	0.397	62.17 \pm 3.25	1.350 \pm 0.072
K 5-1	000.4+04.4	2006 Jul	53.2 \pm 0.6	0.6191 \pm 0.0078	17.34 \pm 0.23	0.074	2.16 \pm 0.19	0.740 \pm 0.075
K 5-11	002.3+02.2	2006 Jul	24.4 \pm 0.3	0.6465 \pm 0.0087	18.22 \pm 0.26	0.000		
K 5-12	353.5-03.3	2006 Jul	246.0 \pm 6.1	1.208 \pm 0.031	35.59 \pm 0.93	0.200		
K 5-14	003.9+02.6	2007 Aug	270.4 \pm 2.1	0.5986 \pm 0.0052	16.50 \pm 0.16	0.087	9.16 \pm 0.19	0.579 \pm 0.014
K 5-17	004.3+02.1	2007 Aug	273.1 \pm 9.2	1.043 \pm 0.037	30.5 \pm 1.1	0.265	9.51 \pm 0.42	1.076 \pm 0.050
K 5-19	005.1+02.0	2007 Aug	56.0 \pm 1.4	1.191 \pm 0.030	35.08 \pm 0.91	0.147	3.49 \pm 0.25	1.275 \pm 0.094
K 5-20	356.8-03.0	2007 Aug	75.5 \pm 1.1	0.639 \pm 0.010	18.02 \pm 0.30	0.121	2.20 \pm 0.16	0.591 \pm 0.049
K 5-3	002.6+05.5	2006 Jul	121.8 \pm 4.0	0.538 \pm 0.020	14.70 \pm 0.59	0.384	5.32 \pm 0.19	0.501 \pm 0.020
K 5-4	351.9-01.9	2006 Jul	363.3 \pm 1.1	0.4946 \pm 0.0016	13.28 \pm 0.05	0.026	20.57 \pm 0.18	0.4922 \pm 0.0049
K 5-5	001.5+03.6	2006 Jul	22.3 \pm 0.3	0.612 \pm 0.011	17.12 \pm 0.31	0.063	3.99 \pm 0.17	0.662 \pm 0.031
K 5-6	003.6+04.9	2006 Jul	62.1 \pm 1.8	0.866 \pm 0.027	25.09 \pm 0.82	0.245	4.73 \pm 0.31	0.927 \pm 0.065
K 5-7	003.1+04.1	2006 Jul	61.5 \pm 1.6	1.323 \pm 0.035	39.1 \pm 1.0	0.157		
K 5-9	355.54-1.4	2006 Jul	22.2 \pm 0.9	0.964 \pm 0.043	28.1 \pm 1.3	0.275	14.19 \pm 0.65	0.932 \pm 0.046
M 1-19	351.1+04.8	2005 May	1142.8 \pm 10.2	0.5640 \pm 0.0056	15.56 \pm 0.17	0.074	48.00 \pm 0.46	0.5540 \pm 0.0059
M 1-20	006.1+08.3	2004 Jun	888.4 \pm 8.0	0.2969 \pm 0.0031	5.97 \pm 0.09	0.120	59.92 \pm 0.62	0.2815 \pm 0.0034
M 1-29	359.1-01.7	2004 Jun	1106.0 \pm 8.0	0.7693 \pm 0.0060	22.08 \pm 0.18	0.059	47.62 \pm 0.63	0.835 \pm 0.012
M 1-31	006.4+02.0	2005 Jul	641.6 \pm 2.9	0.4899 \pm 0.0025	13.11 \pm 0.07	0.049	14.30 \pm 0.23	0.4902 \pm 0.0088
M 1-35	003.9-02.3	2007 Aug	1456.2 \pm 13.3	0.7336 \pm 0.0073	21.03 \pm 0.22	0.082	50.22 \pm 0.48	0.7499 \pm 0.0078
M 1-42	002.7-04.8	2003 Jun	1423.3 \pm 10.4	0.6772 \pm 0.0055	19.21 \pm 0.16	0.096	133.90 \pm 1.05	0.6946 \pm 0.0061
M 1-48	013.4-03.9	2005 Jul	612.4 \pm 4.7	0.5301 \pm 0.0046	14.45 \pm 0.14	0.068	34.17 \pm 0.40	0.5352 \pm 0.0069
M 2-13	011.1+11.5	2006 Jun	925.7 \pm 4.1	0.4008 \pm 0.0020	10.04 \pm 0.06	0.057	59.89 \pm 0.41	0.4043 \pm 0.0032
M 2-15	011.0+06.2	2006 Jun	738.5 \pm 25.6	0.937 \pm 0.035	27.3 \pm 1.0	0.295	37.69 \pm 1.40	0.948 \pm 0.038
M 2-16	357.4-03.2	2004 Jun	1014.5 \pm 9.1	0.7905 \pm 0.0077	22.74 \pm 0.23	0.085	107.34 \pm 0.93	0.7727 \pm 0.0073
M 2-20	000.4-01.9	2006 Jul	862.4 \pm 2.6	0.8262 \pm 0.0027	23.86 \pm 0.08	0.030	48.77 \pm 0.30	0.8514 \pm 0.0056
M 2-21	000.7-02.7	2005 May	2083.6 \pm 54.2	0.945 \pm 0.026	27.52 \pm 0.78	0.205	93.91 \pm 2.43	0.940 \pm 0.026
M 2-22	357.4-04.6	2007 Aug	840.5 \pm 33.5	0.903 \pm 0.039	26.3 \pm 1.2	0.332	14.50 \pm 0.56	0.919 \pm 0.038
M 2-23	002.2-02.7	2004 Jun	2029.5 \pm 10.5	0.5258 \pm 0.0030	14.30 \pm 0.09	0.058	161.07 \pm 0.96	0.5132 \pm 0.0034
M 2-26	003.6-02.3	2006 Jul	204.8 \pm 6.4	1.011 \pm 0.033	29.55 \pm 0.99	0.242	12.06 \pm 0.45	1.034 \pm 0.040
M 2-27	359.9-04.5	2004 Jun	766.9 \pm 5.0	0.6230 \pm 0.0044	17.46 \pm 0.13	0.073	84.78 \pm 0.65	0.6244 \pm 0.0053

TABLE 1 (CONTINUED)

Object	PN G	Run	[O III] λ 5007 deep spectrum				[O III] λ 5007 shallow spectrum	
			Flux (10^3 ADU)	FWHM (\AA)	$\Delta V_{0.5}$ (km/s)	Residual	Flux (10^3 ADU)	FWHM (\AA)
M 2-29	004.0–03.0	2004 Jun	596.8 \pm 4.0	0.4771 \pm 0.0036	12.68 \pm 0.11	0.075	25.44 \pm 0.42	0.4996 \pm 0.0092
M 2-30	003.7–04.6	2004 Jun	1648.5 \pm 28.2	0.864 \pm 0.016	25.02 \pm 0.47	0.149	333.00 \pm 5.66	0.871 \pm 0.016
M 2-31	006.0–03.6	2004 Jun	947.8 \pm 6.4	0.8266 \pm 0.0060	23.87 \pm 0.18	0.062	79.56 \pm 1.13	0.820 \pm 0.013
M 2-33	002.0–06.2	2007 Aug	1051.5 \pm 12.1	0.3441 \pm 0.0046	7.98 \pm 0.14	0.152	107.01 \pm 1.28	0.3456 \pm 0.0048
M 2-39	008.1–04.7	2006 Jul	889.4 \pm 9.5	0.5258 \pm 0.0063	14.31 \pm 0.19	0.129	58.55 \pm 0.73	0.5212 \pm 0.0072
M 2-4	349.8+04.4	2007 Aug	934.8 \pm 5.7	0.5025 \pm 0.0035	13.58 \pm 0.10	0.059	138.62 \pm 0.66	0.4785 \pm 0.0026
M 2-8	352.1+05.1	2006 Jun	1367.9 \pm 4.2	0.6275 \pm 0.0021	17.61 \pm 0.06	0.035	83.45 \pm 0.63	0.6172 \pm 0.0051
M 3-10	358.2+03.6	2004 Jun	2168.0 \pm 18.7	0.7351 \pm 0.0069	21.01 \pm 0.21	0.084		
M 3-14	355.4–02.4	2004 Jun	823.5 \pm 8.1	0.8005 \pm 0.0087	23.06 \pm 0.26	0.114	90.15 \pm 0.95	0.8066 \pm 0.0095
M 3-15	006.8+04.1	2004 Jun	471.4 \pm 4.1	0.647 \pm 0.0062	18.23 \pm 0.19	0.096	24.53 \pm 0.35	0.659 \pm 0.010
M 3-16	359.1–02.3	2005 May	222.6 \pm 2.8	0.6229 \pm 0.0085	17.46 \pm 0.25	0.112	15.46 \pm 0.41	0.652 \pm 0.019
M 3-20	002.1–02.2	2007 Aug	843.4 \pm 4.6	0.7629 \pm 0.0046	21.89 \pm 0.14	0.049	47.46 \pm 0.26	0.7531 \pm 0.0045
M 3-21	355.1–06.9	2004 Jun	1346.5 \pm 12.0	0.5682 \pm 0.0056	15.69 \pm 0.17	0.100	535.43 \pm 4.08	0.57 \pm 0.0049
M 3-26	004.8–05.0	2005 Sep	697.5	1.141	33.54	0.467	11.841.51	0.1822
M 3-32	009.4–09.8	2005 Jul	1309.1 \pm 19.3	0.811 \pm 0.013	23.37 \pm 0.38	0.103	87.49 \pm 1.32	0.793 \pm 0.013
M 3-33	009.6–10.6	2004 Jun	3092.1 \pm 72.3	0.806 \pm 0.020	23.24 \pm 0.61	0.191	107.12 \pm 2.61	0.817 \pm 0.021
M 3-38	356.9+04.4	2004 Jun	321.3 \pm 4.2	0.5289 \pm 0.0077	14.41 \pm 0.23	0.183	15.59 \pm 0.26	0.5348 \pm 0.0098
M 3-42	357.5+03.2	2003 Jun	88.9 \pm 6.0	0.602 \pm 0.046	16.7 \pm 1.4	0.000	16.25 \pm 1.03	1.450 \pm 0.095
M 3-45	359.7–01.8	2005 Jul	243.5 \pm 2.6	0.8117 \pm 0.0095	23.41 \pm 0.28	0.080	23.46 \pm 0.43	0.857 \pm 0.017
M 3-54	018.6–02.2	2006 Jul	387.9 \pm 9.9	0.957 \pm 0.026	27.89 \pm 0.79	0.213	17.76 \pm 0.61	1.005 \pm 0.037
M 4-3	357.2+07.4	2005 May	946.8 \pm 4.0	0.5271 \pm 0.0025	14.35 \pm 0.07	0.055	49.79 \pm 0.34	0.5323 \pm 0.0040
M 4-6	358.6+01.8	2004 Jun	79.6 \pm 1.3	0.772 \pm 0.014	22.15 \pm 0.40	0.120	4.53 \pm 0.32	0.736 \pm 0.057
M 4-7	358.5–02.5	2006 Jun	65.9 \pm 1.0	0.730 \pm 0.012	20.86 \pm 0.36	0.066	3.56 \pm 0.30	0.772 \pm 0.070
PC 12	000.1+17.2	2005 May	151.2 \pm 0.5	0.4749 \pm 0.0019	12.61 \pm 0.06	0.031		
Te 1580	002.6+02.1	2007 Aug	67.5 \pm 3.6	1.367 \pm 0.075	40.4 \pm 2.2	0.380		

simulate the properties of bright extragalactic planetary nebulae in environments without star formation. As discussed in more detail in Richer et al. (2008), our selection criteria quickly converged to require the planetary nebulae (a) lie within 10° of the galactic centre, (b) have a large reddening-corrected $H\beta$ flux, nominally $\log I(H\beta) > -12.0$ dex, (c) have a large $[O III]\lambda 5007/H\beta$ ratio, normally exceeding a value of 6, and (d) have been observed spectroscopically at low resolution with a detection of the $[O III]\lambda 4363$ line. Our Bulge sample contains 86 objects.

We acquired our observations of Bulge planetary nebulae during eight observing runs spanning the period from 2003 June to 2007 August at the Observatorio Astronómico Nacional in the Sierra San Pedro Mártir, Baja California, Mexico (OAN-SPM). All of these objects were selected from existing spectroscopic surveys (Aller & Keyes 1987; Webster 1988; Cuisinier, Acker, & Köppen 1996; Ratag et al. 1997; Cuisinier et al. 2000; Escudero & Costa 2001; Escudero, Costa, & Maciel 2004; Exter, Barlow, & Walton 2004; Górny et al. 2004). Some of our observations of extragalactic planetary nebulae were acquired during the same runs, but also during three additional observing runs in 2001 September, 2002 July, and 2004 November. More details of the observations will be provided elsewhere (López et al.

2009, in preparation; Richer et al. 2009, in preparation).

High resolution spectra were obtained with the Manchester echelle spectrometer (MES-SPM; Meaburn et al. 1984, 2003). The MES-SPM is a long slit echelle spectrometer, but uses narrow-band filters, instead of a cross-disperser, to isolate the orders containing emission lines of interest. In this case, filters isolated orders 87 and 114 containing the $H\alpha$ and $[O III]\lambda 5007$ emission lines, respectively. All observations used a $150 \mu\text{m}$ wide slit, equivalent to $1''.9$ on the sky. Coupled with a SITe 1024×1024 CCD with $24 \mu\text{m}$ pixels binned 2×2 , the resulting spectral resolutions were approximately $0.077 \text{\AA}/\text{pix}$ and $0.100 \text{\AA}/\text{pix}$ at $[O III]\lambda 5007$ and $H\alpha$, respectively (equivalent to 11 km s^{-1} for 2.6 pix FWHM). Immediately before or after every object spectrum, exposures of a ThAr lamp were taken to calibrate in wavelength. The internal precision of the arc lamp calibrations is better than $\pm 1.0 \text{ km s}^{-1}$.

Typically, three spectra were obtained of each Bulge planetary nebula. The first spectrum was a short exposure in $[O III]\lambda 5007$ with a duration of 60–180s. This was followed by a deep $[O III]\lambda 5007$ spectrum, up to a maximum of 30 minutes, but chosen so as to avoid saturation. The last spectrum was a deep $H\alpha$ spectrum, whose exposure time was chosen to achieve a S/N similar to that of the deep

TABLE 2
DEEP H α AND SIMULATED EXTRAGALACTIC SPECTRA

Object	PN G	Deep H α spectrum				[O III] λ 5007 sim x-gal spectrum		
		Flux (10^3 ADU)	FWHM (\AA)	$\Delta V_{0.5}$ (km s^{-1})	Residual	$I(6560)/I(\text{H}\alpha)$	Flux (10^3 ADU)	FWHM (\AA)
Bl 3-13	000.9-02.0	911.8 \pm 2.4	0.9427 \pm 0.0028	16.05 \pm 0.06	0.025		5.21 \pm 0.16	0.607 \pm 0.021
Cn 1-5	002.2-09.4	1899.7 \pm 4.3	1.0384 \pm 0.0026	18.87 \pm 0.06	0.029		5.45 \pm 0.27	1.248 \pm 0.064
Cn 2-1	356.2-04.4	175.5 \pm 0.7	0.9255 \pm 0.0039	15.51 \pm 0.09	0.027		5.08 \pm 0.15	0.678 \pm 0.023
H 1-1	343.4+11.9	1291.7 \pm 14.2	1.617 \pm 0.0186	34.04 \pm 0.43	0.103	0.0105 \pm 0.0088	5.17 \pm 0.28	1.205 \pm 0.067
H 1-11	002.6+08.2	1245.2 \pm 7.0	0.9219 \pm 0.0057	15.40 \pm 0.13	0.054	0.0039 \pm 0.0046	5.23 \pm 0.15	0.626 \pm 0.019
H 1-14	001.7+05.7	664.7 \pm 12.5	1.8033 \pm 0.0355	38.62 \pm 0.81	0.175	0.0094 \pm 0.0153	5.36 \pm 0.33	1.303 \pm 0.083
H 1-16	000.1+04.3	1447.8 \pm 3.9	1.0257 \pm 0.003	18.51 \pm 0.07	0.023	0.0100 \pm 0.0022	5.19 \pm 0.15	0.728 \pm 0.023
H 1-17	358.3+03.0	1022.5 \pm 3.4	0.9635 \pm 0.0035	16.67 \pm 0.08	0.032		5.29 \pm 0.15	0.622 \pm 0.019
H 1-18	357.6+02.6	1218.8 \pm 3.5	0.8105 \pm 0.0026	11.67 \pm 0.06	0.041	0.0003 \pm 0.0023	5.09 \pm 0.13	0.498 \pm 0.015
H 1-20	358.9+03.2	960.1 \pm 2.4	0.9361 \pm 0.0025	15.85 \pm 0.06	0.019		4.71 \pm 0.16	0.690 \pm 0.025
H 1-23	357.6+01.7	502.3 \pm 3.6	1.0266 \pm 0.008	18.54 \pm 0.18	0.069		5.20 \pm 0.18	0.760 \pm 0.030
H 1-27	005.0+04.4	1264.4 \pm 3.2	1.0238 \pm 0.0029	18.48 \pm 0.07	0.026		5.23 \pm 0.16	0.730 \pm 0.024
H 1-30	352.0-04.6	665.5 \pm 2.8	0.9616 \pm 0.0044	16.62 \pm 0.10	0.047	0.0101 \pm 0.0034	5.29 \pm 0.15	0.605 \pm 0.018
H 1-31	355.1-02.9	904.8 \pm 3.1	0.9932 \pm 0.0037	17.56 \pm 0.08	0.034	0.0020 \pm 0.0028	5.12 \pm 0.14	0.646 \pm 0.019
H 1-32	355.6-02.7	2318.3 \pm 7.0	0.7685 \pm 0.0026	10.08 \pm 0.06	0.039		5.09 \pm 0.13	0.435 \pm 0.012
H 1-33	355.7-03.0	1339.9 \pm 2.7	0.7904 \pm 0.0018	10.93 \pm 0.04	0.013		5.22 \pm 0.13	0.527 \pm 0.015
H 1-40	359.7-02.6	163.5 \pm 2.1	1.0137 \pm 0.0142	18.16 \pm 0.32	0.126		5.14 \pm 0.18	0.616 \pm 0.024
H 1-41	356.7-04.8	1655.8 \pm 12.0	1.1607 \pm 0.0091	22.30 \pm 0.21	0.066	0.0148 \pm 0.0058	5.34 \pm 0.20	0.852 \pm 0.035
H 1-42	357.2-04.5	1558.4 \pm 8.9	0.9351 \pm 0.0059	15.81 \pm 0.13	0.068		5.20 \pm 0.15	0.544 \pm 0.017
H 1-45	002.0-02.0	1429.3 \pm 9.7	1.5897 \pm 0.0113	33.37 \pm 0.26	0.055	0.0223 \pm 0.0055	5.27 \pm 0.19	1.007 \pm 0.038
H 1-50	358.7-05.2	2058.0 \pm 3.3	1.0263 \pm 0.0018	18.53 \pm 0.04	0.021	0.0074 \pm 0.0013	5.09 \pm 0.15	0.696 \pm 0.023
H 1-54	002.1-04.2	3220.8 \pm 14.6	0.9029 \pm 0.0045	14.81 \pm 0.10	0.047		5.36 \pm 0.13	0.545 \pm 0.015
H 1-56	001.7-04.6	1157.9 \pm 1.6	0.8261 \pm 0.0013	12.25 \pm 0.03	0.015		5.35 \pm 0.15	0.563 \pm 0.018
H 1-59	003.8-04.3	302.9 \pm 3.4	1.2366 \pm 0.0147	24.33 \pm 0.34	0.091	0.0408 \pm 0.0092	5.33 \pm 0.24	1.138 \pm 0.053
H 1-60	004.2-04.3	680.2 \pm 4.9	0.956 \pm 0.0076	16.45 \pm 0.17	0.063		5.29 \pm 0.16	0.693 \pm 0.023
H 1-67	009.8-04.6	1278.4 \pm 25.0	1.4737 \pm 0.0297	30.46 \pm 0.68	0.169	0.0395 \pm 0.0160	4.27 \pm 0.21	0.657 \pm 0.036
H 2-10	358.2+03.5	222.9 \pm 1.7	1.1028 \pm 0.0093	20.70 \pm 0.21	0.055		5.32 \pm 0.17	0.811 \pm 0.029
H 2-11	000.7+04.7	64.5 \pm 0.4	0.7697 \pm 0.0058	10.13 \pm 0.13	0.038		5.31 \pm 0.14	0.499 \pm 0.014
H 2-18	006.3+04.4	717.5 \pm 9.4	1.4733 \pm 0.0204	30.44 \pm 0.47	0.125	0.0043 \pm 0.0105	5.34 \pm 0.22	1.151 \pm 0.050
Hb 8	003.8-17.1	1553.2 \pm 3.2	0.9662 \pm 0.0022	16.75 \pm 0.05	0.024		4.92 \pm 0.14	0.617 \pm 0.020
He 2-250	000.7+03.2	287.4 \pm 5.1	1.1849 \pm 0.0211	22.96 \pm 0.48	0.117	0.0313 \pm 0.0153	4.94 \pm 0.19	0.771 \pm 0.032
Hf 2-1	355.4-04.0	759.4 \pm 24.6	1.7739 \pm 0.059	37.91 \pm 1.35	0.281	0.0876 \pm 0.0266	5.23 \pm 0.35	1.318 \pm 0.091
K 5-1	000.4+04.4	264.7 \pm 0.7	0.8709 \pm 0.0027	13.76 \pm 0.06	0.021		5.17 \pm 0.16	0.602 \pm 0.020
K 5-11	002.3+02.2	96.3 \pm 0.5	0.9577 \pm 0.0054	16.51 \pm 0.12	0.000		5.17 \pm 0.15	0.624 \pm 0.020
K 5-12	353.5-03.3	255.2 \pm 2.6	1.548 \pm 0.0166	32.33 \pm 0.38	0.094	0.0396 \pm 0.0083	4.92 \pm 0.26	1.193 \pm 0.065
K 5-14	003.9+02.6	155.1 \pm 1.2	1.0314 \pm 0.0087	18.69 \pm 0.20	0.075	0.0114 \pm 0.0063	4.99 \pm 0.14	0.632 \pm 0.019
K 5-17	004.3+02.1	509.9 \pm 9.1	1.4345 \pm 0.0271	29.48 \pm 0.62	0.172	0.0120 \pm 0.0145	4.60 \pm 0.23	1.042 \pm 0.055
K 5-19	005.1+02.0	111.5 \pm 1.2	1.4087 \pm 0.0157	28.81 \pm 0.36	0.075	0.0517 \pm 0.0086	5.38 \pm 0.25	1.219 \pm 0.060
K 5-20	356.8-03.0	161.9 \pm 0.9	0.9118 \pm 0.0054	15.09 \pm 0.12	0.044		5.34 \pm 0.15	0.646 \pm 0.020
K 5-3	002.6+05.5	234.7 \pm 6.6	1.3682 \pm 0.041	27.77 \pm 0.94	0.260	0.0356 \pm 0.0227	4.56 \pm 0.19	0.448 \pm 0.021
K 5-4	351.9-01.9	1422.2 \pm 2.1	0.8187 \pm 0.0013	11.97 \pm 0.03	0.016		5.15 \pm 0.13	0.512 \pm 0.014
K 5-5	001.5+03.6	119.9 \pm 0.5	0.9265 \pm 0.0047	15.54 \pm 0.11	0.025		5.28 \pm 0.16	0.625 \pm 0.021
K 5-6	003.6+04.9	86.5 \pm 1.1	1.3015 \pm 0.0182	26.04 \pm 0.42	0.089	0.0245 \pm 0.0105	5.25 \pm 0.23	0.883 \pm 0.042
K 5-7	003.1+04.1	55.6 \pm 0.7	1.6188 \pm 0.0227	32.49 \pm 0.52	0.080	0.0294 \pm 0.0108	5.10 \pm 0.26	1.279 \pm 0.067
K 5-9	355.54-1.4	156.7 \pm 4.0	1.2893 \pm 0.0354	25.72 \pm 0.81	0.220	0.0185 \pm 0.0207	4.94 \pm 0.29	0.942 \pm 0.059
M 1-19	351.1+04.8	1619.8 \pm 3.8	0.8781 \pm 0.0022	14.00 \pm 0.05	0.021		5.22 \pm 0.13	0.575 \pm 0.016
M 1-20	006.1+08.3	3164.6 \pm 13.7	0.7527 \pm 0.0037	9.43 \pm 0.08	0.055		5.19 \pm 0.11	0.3048 \pm 0.0073
M 1-29	359.1-01.7	2186.2 \pm 6.5	1.0319 \pm 0.0033	18.69 \pm 0.08	0.027	0.0154 \pm 0.0024	5.36 \pm 0.16	0.778 \pm 0.025
M 1-31	006.4+02.0	2958.7 \pm 14.8	0.7954 \pm 0.0044	11.11 \pm 0.10	0.049		5.22 \pm 0.12	0.471 \pm 0.012
M 1-35	003.9-02.3	3276.4 \pm 18.3	1.0215 \pm 0.0063	18.40 \pm 0.14	0.056		5.42 \pm 0.17	0.721 \pm 0.025
M 1-42	002.7-04.8	3097.7 \pm 10.2	1.0485 \pm 0.0038	19.18 \pm 0.09	0.055	0.0056 \pm 0.0026	5.31 \pm 0.16	0.684 \pm 0.023
M 1-48	013.4-03.9	974.1 \pm 2.5	0.8262 \pm 0.0024	12.23 \pm 0.05	0.026	0.0057 \pm 0.0021	5.03 \pm 0.14	0.541 \pm 0.017
M 2-13	011.1+11.5	1556.5 \pm 5.0	0.7047 \pm 0.0025	7.25 \pm 0.06	0.042		5.24 \pm 0.11	0.3992 \pm 0.0094
M 2-15	011.0+06.2	1080.0 \pm 22.1	1.2705 \pm 0.0278	25.23 \pm 0.64	0.194	0.0160 \pm 0.0164	5.28 \pm 0.25	0.927 \pm 0.046
M 2-16	357.4-03.2	1508.6 \pm 7.3	1.109 \pm 0.0057	20.87 \pm 0.13	0.041	0.0093 \pm 0.0040	5.22 \pm 0.16	0.780 \pm 0.026
M 2-20	000.4-01.9	1417.2 \pm 4.3	1.2428 \pm 0.0041	24.50 \pm 0.09	0.026		5.33 \pm 0.17	0.845 \pm 0.023
M 2-21	000.7-02.7	1497.2 \pm 18.2	1.2804 \pm 0.0164	25.49 \pm 0.37	0.108	0.0148 \pm 0.0098	5.02 \pm 0.21	0.947 \pm 0.043
M 2-22	357.4-04.6	481.5 \pm 10.7	1.2341 \pm 0.0295	24.27 \pm 0.67	0.205	0.0223 \pm 0.0179	5.37 \pm 0.27	0.919 \pm 0.050
M 2-23	002.2-02.7	2511.1 \pm 5.7	0.855 \pm 0.0021	13.22 \pm 0.05	0.023		4.91 \pm 0.14	0.539 \pm 0.017
M 2-26	003.6-02.3	543.1 \pm 9.4	1.3191 \pm 0.0244	26.50 \pm 0.56	0.164	0.0196 \pm 0.0140	5.28 \pm 0.25	1.014 \pm 0.050
M 2-27	359.9-04.5	2440.0 \pm 7.8	0.9625 \pm 0.0034	16.64 \pm 0.08	0.046		4.96 \pm 0.14	0.624 \pm 0.020

TABLE 2 (CONTINUED)

Object	PN G	Deep H α spectrum				[O III] λ 5007 sim x-gal spectrum		
		Flux (10^3 ADU)	FWHM (\AA)	$\Delta V_{0.5}$ (km s $^{-1}$)	Residual	$I(6560)/I(\text{H}\alpha)$	Flux (10^3 ADU)	FWHM (\AA)
M 2-29	004.0-03.0	2212.0 \pm 6.6	0.7864 \pm 0.0026	10.77 \pm 0.06	0.060		5.27 \pm 0.13	0.489 \pm 0.013
M 2-30	003.7-04.6	2473.0 \pm 21.5	1.1838 \pm 0.0108	22.91 \pm 0.25	0.071	0.0261 \pm 0.0069	4.82 \pm 0.19	0.853 \pm 0.036
M 2-31	006.0-03.6	2982.6 \pm 15.8	1.1907 \pm 0.0068	23.10 \pm 0.16	0.056		4.92 \pm 0.16	0.811 \pm 0.029
M 2-33	002.0-06.2	1398.1 \pm 5.6	0.6988 \pm 0.0031	6.98 \pm 0.07	0.050		5.18 \pm 0.12	0.3379 \pm 0.0092
M 2-39	008.1-04.7	2037.2 \pm 9.5	1.0341 \pm 0.0053	18.76 \pm 0.12	0.096		5.31 \pm 0.14	0.542 \pm 0.016
M 2-4	349.8+04.4	1660.4 \pm 7.6	0.8088 \pm 0.0041	11.63 \pm 0.09	0.047		5.03 \pm 0.13	0.480 \pm 0.014
M 2-8	352.1+05.1	2316.7 \pm 4.2	0.9742 \pm 0.0019	17.00 \pm 0.04	0.028	0.0104 \pm 0.0015	5.34 \pm 0.15	0.662 \pm 0.020
M 3-10	358.2+03.6	4224.1 \pm 31.0	1.0963 \pm 0.0085	20.52 \pm 0.19	0.059	0.0094 \pm 0.0061	5.40 \pm 0.16	0.762 \pm 0.024
M 3-14	355.4-02.4	1998.8 \pm 12.1	1.1585 \pm 0.0075	22.23 \pm 0.17	0.066	0.0089 \pm 0.0050	5.24 \pm 0.18	0.811 \pm 0.030
M 3-15	006.8+04.1	1305.8 \pm 3.9	0.9783 \pm 0.0033	17.12 \pm 0.08	0.052		5.30 \pm 0.16	0.651 \pm 0.021
M 3-16	359.1-02.3	548.6 \pm 3.6	1.0279 \pm 0.0074	18.58 \pm 0.17	0.060		5.40 \pm 0.15	0.657 \pm 0.021
M 3-20	002.1-02.2	848.9 \pm 6.5	1.1206 \pm 0.0093	21.20 \pm 0.21	0.069		5.27 \pm 0.15	0.763 \pm 0.025
M 3-21	355.1-06.9	450.3 \pm 2.8	0.8936 \pm 0.0062	14.49 \pm 0.14	0.068		5.18 \pm 0.14	0.584 \pm 0.018
M 3-26	004.8-05.0	928.6 \pm 31.3	1.4618 \pm 0.0519	30.16 \pm 1.19	0.304	0.0202 \pm 0.0271	5.35 \pm 0.40	1.173 \pm 0.090
M 3-32	009.4-09.8	3166.9 \pm 29.4	1.1757 \pm 0.0118	22.70 \pm 0.27	0.083	0.0103 \pm 0.0075	5.32 \pm 0.18	0.837 \pm 0.031
M 3-33	009.6-10.6	2168.7 \pm 22.1	1.0977 \pm 0.0122	20.55 \pm 0.28	0.096	0.0149 \pm 0.0082	4.92 \pm 0.23	0.798 \pm 0.040
M 3-38	356.9+04.4	442.8 \pm 3.7	0.9558 \pm 0.0086	16.44 \pm 0.20	0.120	0.0108 \pm 0.0068	5.00 \pm 0.15	0.526 \pm 0.017
M 3-42	357.5+03.2	240.8 \pm 14.6	1.7103 \pm 0.0955	36.35 \pm 2.18	0.332	0.0384 \pm 0.0562	5.11 \pm 0.36	1.47 \pm 0.11
M 3-45	359.7-01.8	422.8 \pm 2.3	1.1658 \pm 0.0068	22.43 \pm 0.16	0.043	0.0197 \pm 0.0044	5.19 \pm 0.15	0.806 \pm 0.025
M 3-54	018.6-02.2	728.4 \pm 10.3	1.3395 \pm 0.02	27.03 \pm 0.46	0.138	0.0315 \pm 0.0114	4.84 \pm 0.22	0.952 \pm 0.046
M 4-3	357.2+07.4	1918.1 \pm 4.6	0.8502 \pm 0.0022	13.07 \pm 0.05	0.031		5.06 \pm 0.13	0.501 \pm 0.015
M 4-6	358.6+01.8	255.3 \pm 1.4	1.1311 \pm 0.0067	21.48 \pm 0.15	0.046		5.21 \pm 0.18	0.835 \pm 0.032
M 4-7	358.5-02.5	175.2 \pm 0.9	1.0558 \pm 0.006	19.38 \pm 0.14	0.017		4.86 \pm 0.16	0.678 \pm 0.025
PC 12	000.1+17.2	1820.5 \pm 3.7	0.8346 \pm 0.0019	12.53 \pm 0.04	0.033		5.24 \pm 0.12	0.487 \pm 0.013
Te 1580	002.6+02.1	140.9 \pm 4.6	1.8833 \pm 0.0647	40.58 \pm 1.48	0.277	0.0136 \pm 0.0269	4.97 \pm 0.35	1.310 \pm 0.095

[O III] λ 5007 spectrum, though it was also limited to a maximum of 30 minutes duration. The purpose of the short [O III] λ 5007 spectrum was to attempt to simulate the S/N in typical spectra of extragalactic planetary nebulae. The deep [O III] λ 5007 and H α spectra were obtained so as to detect kinematic details that are unobservable in typical spectra of extragalactic planetary nebulae. For the extragalactic planetary nebulae, all of the spectra were of 30 minutes duration and, depending upon the S/N, one or two spectra were obtained. It was not always possible to obtain multiple spectra during a single pointing.

All of the Bulge planetary nebulae are resolved (Richer et al. 2008). In all cases, we attempted to center the slit on the object as carefully as possible (see the top image in Figure 1). Normally, all of the spectra for a given object were obtained sequentially, which should help minimize positional mismatches. For the extragalactic planetary nebulae, the slit was always oriented in the north-south direction, as it was for the vast majority of Bulge planetary nebulae.

All of the spectra were reduced using the twodspec and specred packages of the Image Reduction and Analysis Facility⁴ (IRAF). For the Bulge ob-

jects, the data reduction followed the scheme recommended by Massey, Valdes, & Barnes (1992, Appendix B) for long slit spectroscopy. We edited each spectrum of cosmic rays. Then, we subtracted a nightly mean bias image from each object spectrum. Next, we mapped positions of constant wavelength using the arc lamp spectra. We then rectified the object spectra so that lines of constant wavelength fell exactly along the columns, a process that simultaneously applied a wavelength calibration (see the two-dimensional spectrum in Figure 1). Finally, we extracted wavelength-calibrated, one-dimensional spectra for each object (see the one-dimensional spectrum in Figure 1). We did not calibrate in flux.

For the extragalactic planetary nebulae, the data reduction followed that outlined above for cosmic rays and bias. We then extracted the source spectra and used these apertures to extract ThAr spectra from the lamp spectra. The latter were used to calibrate in wavelength. If two spectra were obtained, they were co-added after being calibrated in wavelength. If they did not coincide exactly in wavelength, they were shifted to a common wavelength solution and then co-added. Again, we did not calibrate in flux.

⁴IRAF is distributed by the National Optical Astronomical Observatories, which is operated by the Associated Universities for Research in Astronomy, Inc., under contract to the

National Science Foundation.

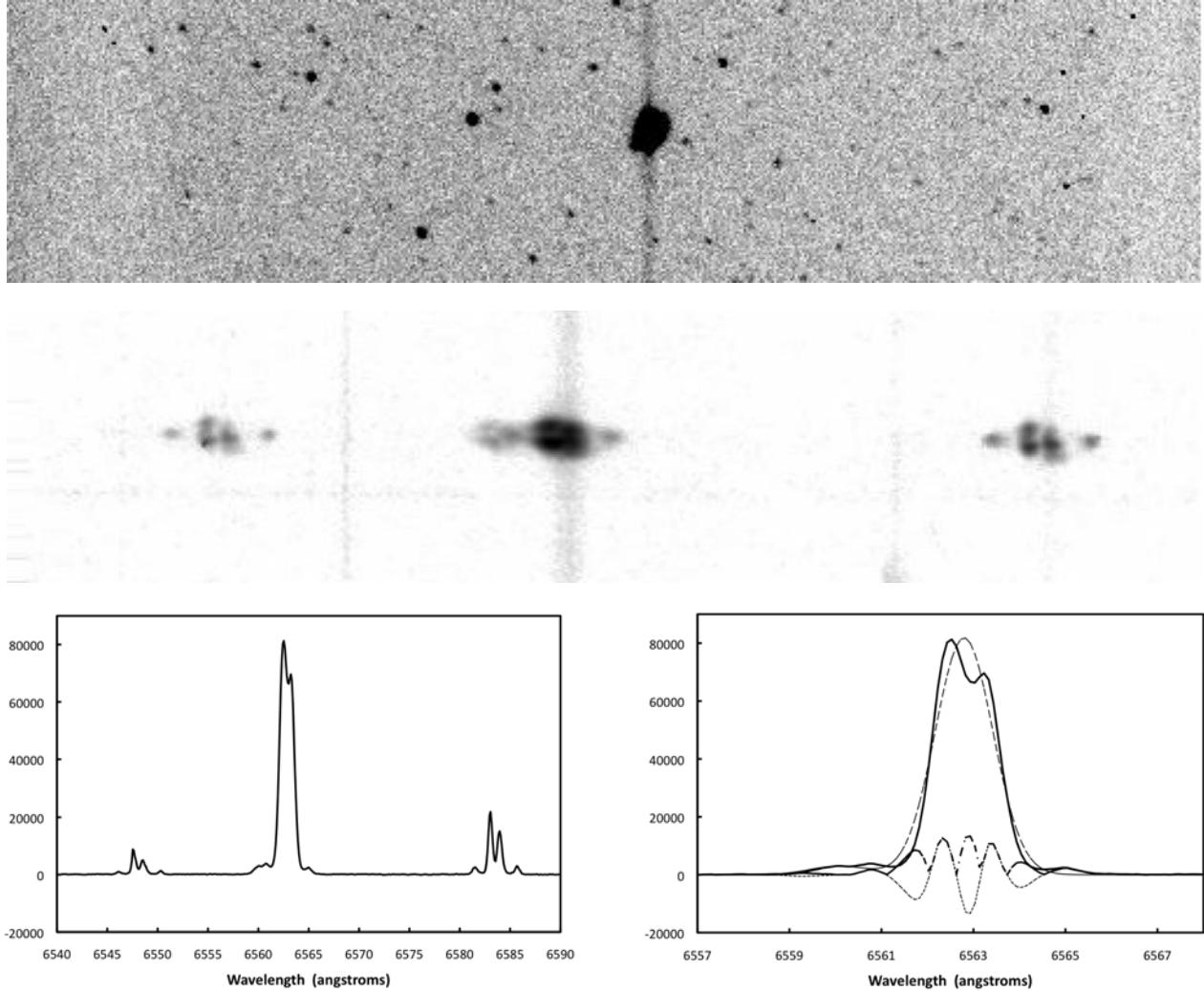


Fig. 1. We illustrate the analysis of our spectra using H 1-67 as an example. The top image is the acquisition image, showing the slit superposed upon the object (north is up; east to the left). The middle image is the rectified two-dimensional $H\alpha$ spectrum (north is up; blue to the left). The structure of the $H\alpha$ line differs from that in the $[N II]\lambda\lambda 6548, 6583$ lines because it is blended with $He II\lambda 6560$. At lower left is the extracted, wavelength-calibrated, spatially unresolved, one-dimensional spectrum. Finally, at lower right is the extracted spectrum (solid line), the fit of a single Gaussian component to the $H\alpha$ and $He II\lambda 6560$ lines (dashed line), the difference between the extracted spectrum and the fit (lower dotted line), and the absolute value of this difference (lower dot-dashed line). The residual flux about the Gaussian fit is the sum of the flux under the dot-dashed line, and, for H 1-67, represents 17% of the flux in the Gaussian component fit to the $H\alpha$ line. For both 1-D spectra, the ordinate is in units of counts.

Figures 2–9 present the one-dimensional line profiles for all of the objects in our sample. For the Bulge planetary nebulae, we present the shallow and deep $[O III]\lambda 5007$ spectra as well as the $H\alpha$ spectra. For the extragalactic planetary nebulae, we present the spectra in both $[O III]\lambda 5007$ and $H\alpha$.

3. ANALYSIS OF THE LINE PROFILES

The line profiles of extragalactic planetary nebulae usually cannot be distinguished statistically from

a Gaussian shape (Dopita et al. 1985, 1988; Zijlstra et al. 2006; Arnaboldi et al. 2008, see also Figure 9). While it may be somewhat surprising, the majority of the line profiles for the Bulge planetary nebulae in Figures 2–9 are not too different from a Gaussian in shape. These observations motivate the analysis that follows.

We analyzed the one-dimensional line profiles with a locally-implemented software package (IN-

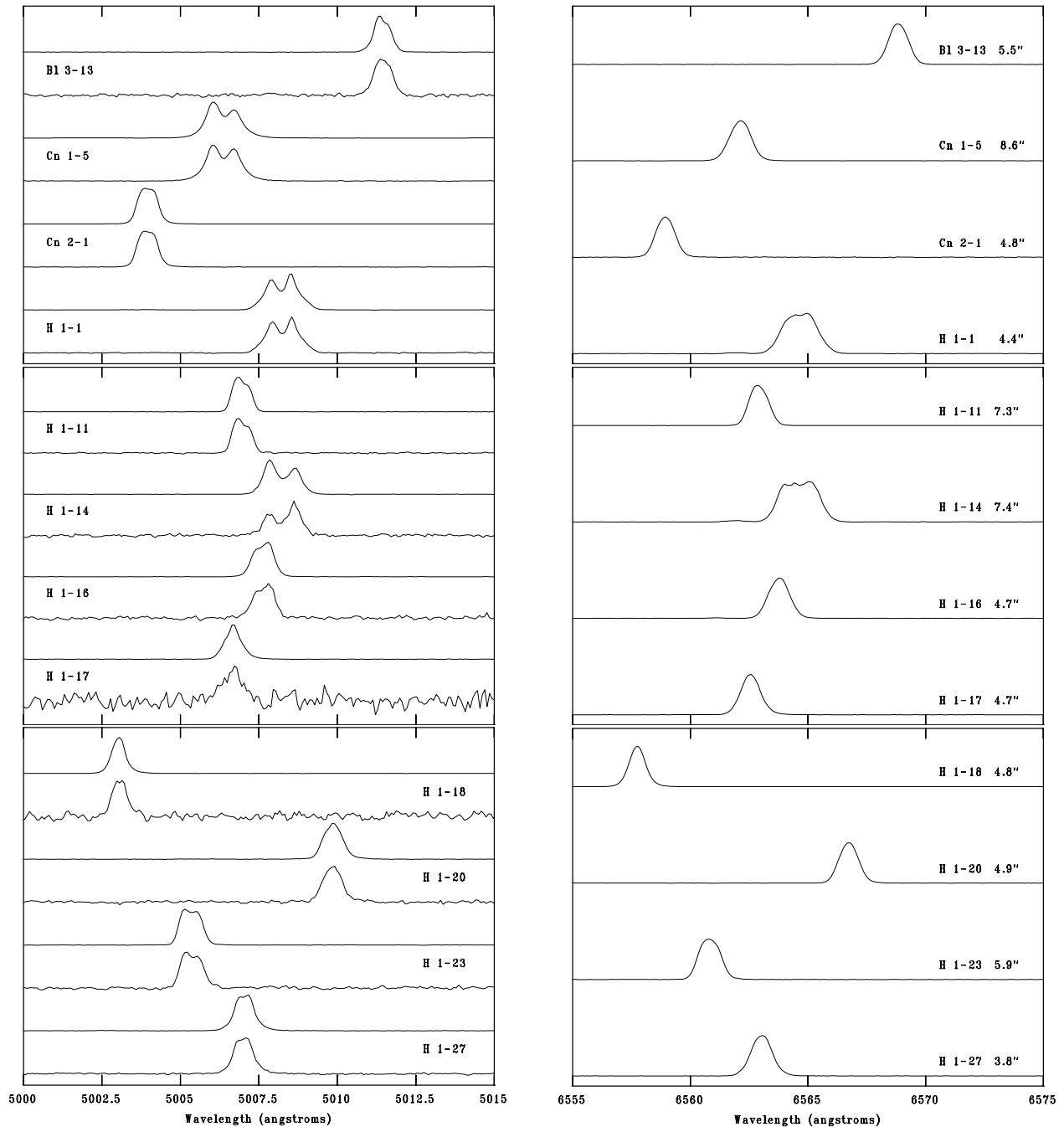


Fig. 2. We present the line profiles for our sample of planetary nebulae. When both deep and shallow [O III] $\lambda 5007$ spectra are available, both are shown (the shallow spectrum below the deep one). Note how similar the two [O III] $\lambda 5007$ spectra are. At this scaling, the He II $\lambda 6560$ line is not easily visible in the H α spectra. The wavelength scales are common in each column. The H α panels include the diameter at 10% of peak intensity from Richer et al. (2008).

TENS; McCall, Rybski, & Shields 1985) to determine the radial velocity, flux, and profile width (FWHM; full width at half maximum intensity) as well as the uncertainties (1σ) in these parameters. This software fits the emission line profile with a

sampled Gaussian function and models the continuum as a straight line (see the last panel in Figure 1). Thus, this analysis assumes that the lines have a Gaussian shape and that they are superposed on a flat continuum. In the case of the H α line, the

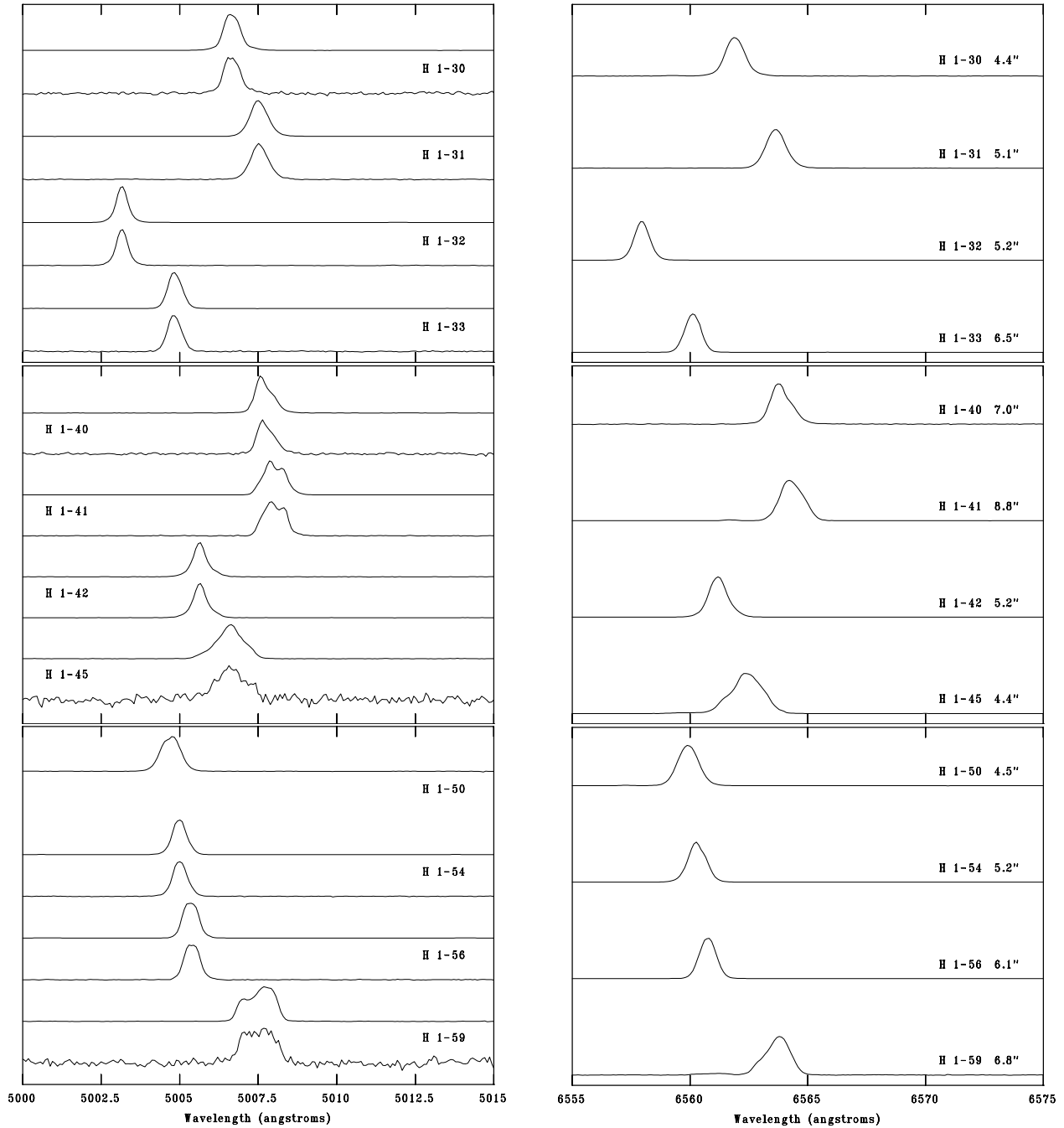


Fig. 3. For H 1-50, only a deep [O III]λ5007 spectrum was obtained. See Figure 2 for further details.

He II λ6560 line may also be present. In this case, a fit is made simultaneously to both lines and the continuum, but assuming that the widths of both lines are identical.

In addition to analysing all of the observed spectra of the Bulge planetary nebulae with INTENS, we also used them to construct synthetic [O III]λ5007 spectra of extragalactic planetary nebulae. To con-

struct these synthetic spectra, we re-normalized each deep [O III]λ5007 spectrum of our Bulge planetary nebulae to the total flux typically observed in bright extragalactic planetary nebulae, about 5300 counts (Richer et al. 2009, in preparation). We then added a typical extragalactic background continuum spectrum to these re-normalized spectra. (The background used was that for the Fornax PN, once the

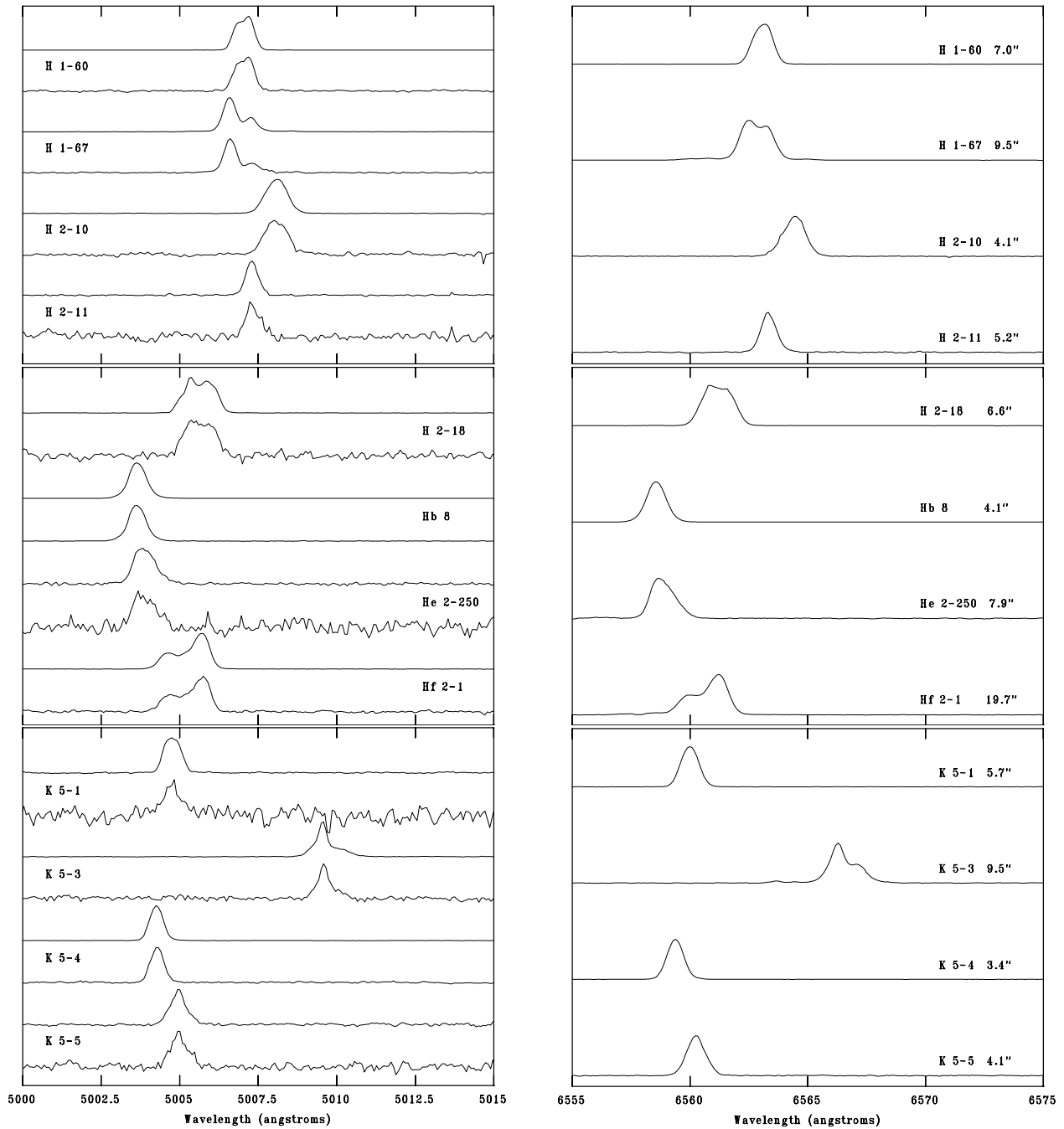


Fig. 4. See Figure 2 for further details.

emission line was removed.) We then analysed these synthetic spectra with INTENS in the same way as for the observed spectra. Figures 1 and 10 demonstrate this transformation and analysis for H 1-67 and H 1-41, respectively.

We end our analysis of the deep H α and [O III] λ 5007 spectra by determining the flux that is not represented by the Gaussian fit. To obtain this

residual flux, we subtract the Gaussian fit from the original line profile, take the absolute value of the residual, and sum the residual over the line. This procedure measures the flux that deviates from a Gaussian line profile. Figures 1 and 11 illustrate this procedure for H 1-67 and H 1-41, respectively. Since extragalactic planetary nebulae have line profiles that are approximately Gaussian in shape (Fig-

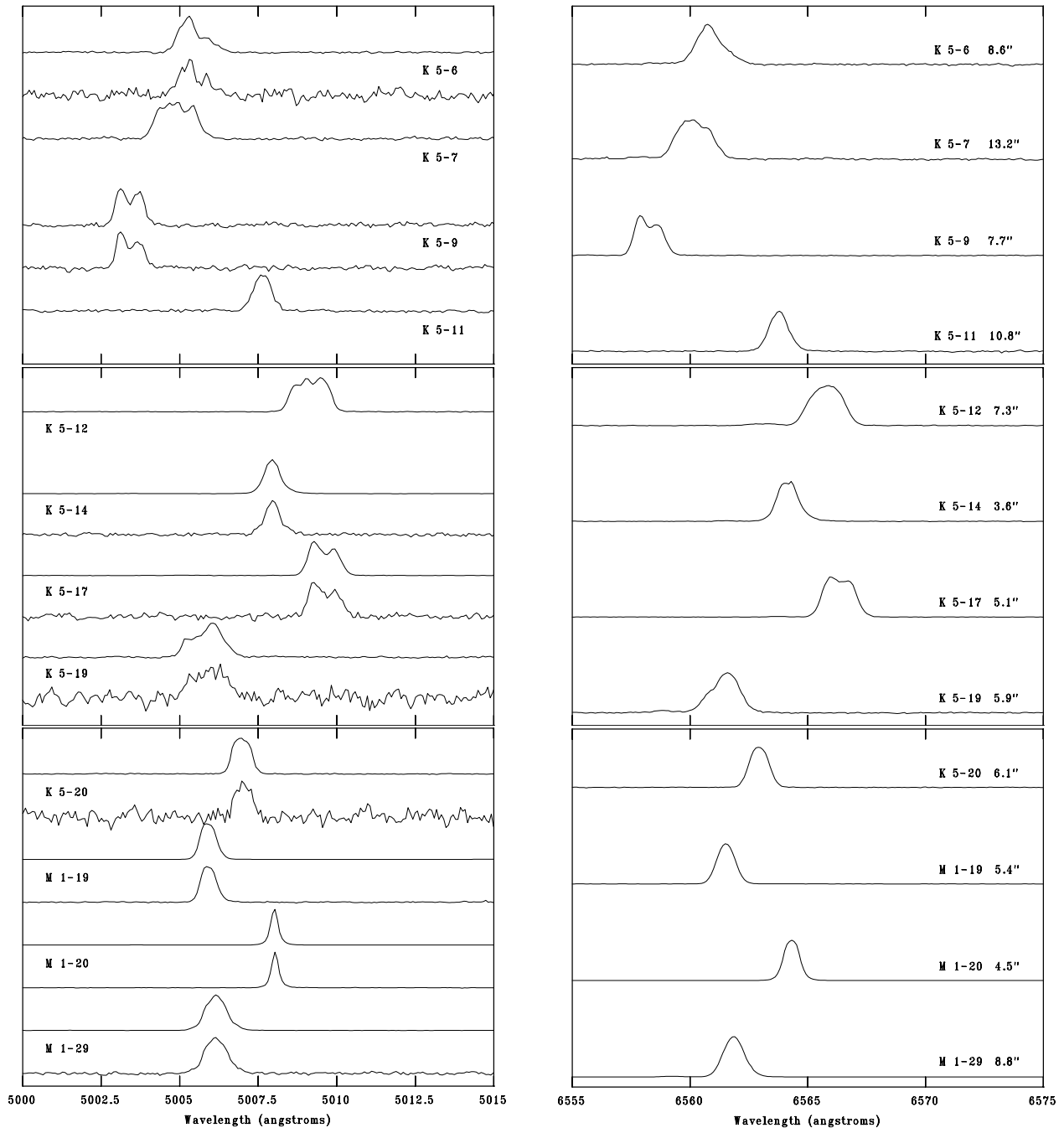


Fig. 5. For K 5-7 and K 5-12, only a deep [O III] $\lambda 5007$ spectrum was obtained. See Figure 2 for further details.

ure 9, also Dopita et al. 1985, 1988; Arnaboldi et al. 2008), our intention here is to estimate the fraction of the flux in our deep observations of Bulge planetary nebulae that would be missed in observations of extragalactic planetary nebulae.

Clearly, a Gaussian function will be a poor approximation to the shape of the double-peaked line profiles in Figures 2-9. However, even for those

cases, the FWHM of the Gaussian is similar to the separation of the outer 50% intensity points for the two peaks, except when the line profiles are very asymmetric. This would not have been the case had we adopted a width based upon some lower intensity fraction, such as the 10% that is often adopted (e.g., Dopita et al. 1985, 1988). Since our goal is to retain an analysis as close to the method we would

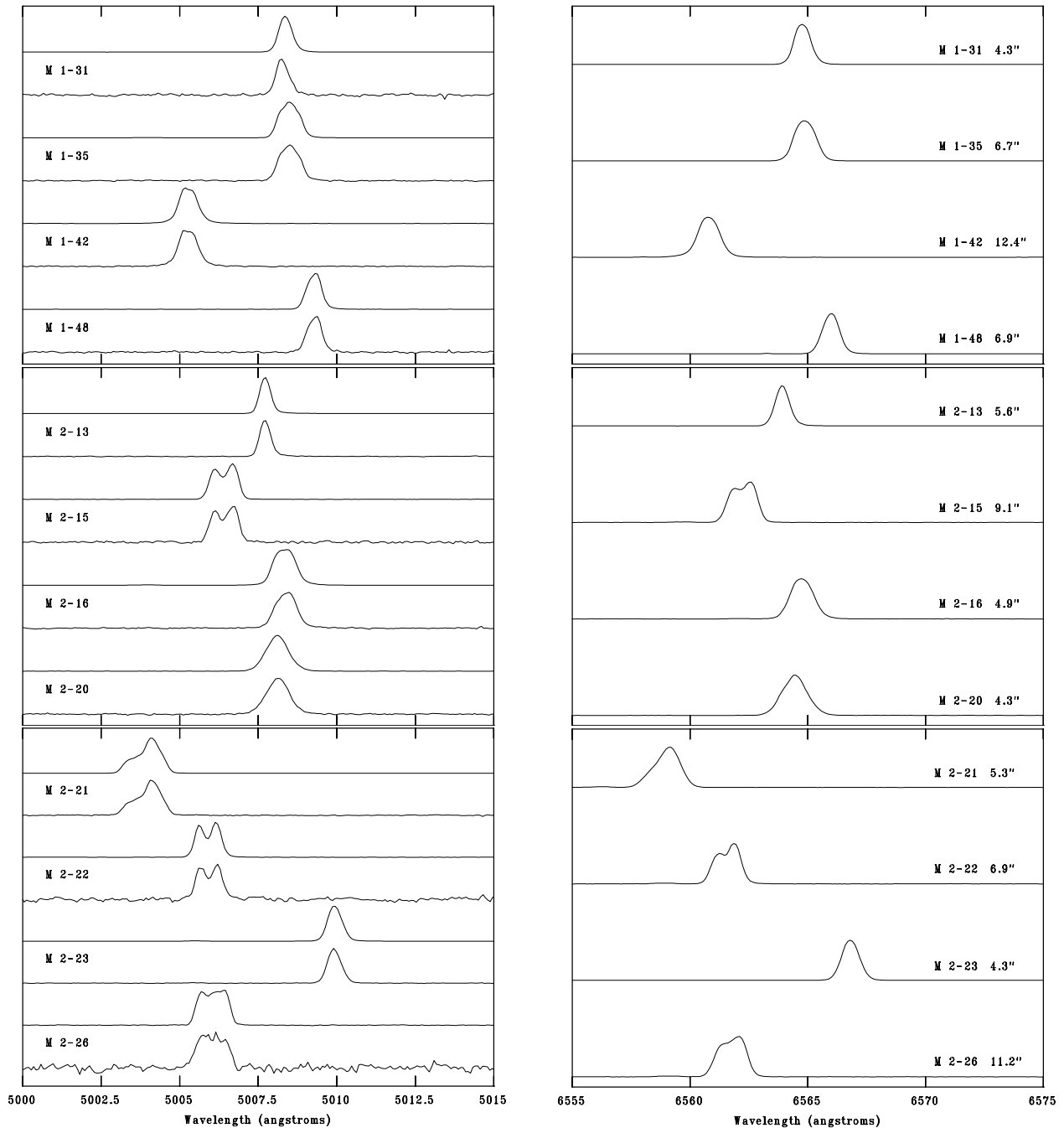


Fig. 6. See Figure 2 for further details.

employ for extragalactic planetary nebulae, whose line profiles are nearly Gaussian, we have refrained from applying a double-Gaussian fit to the double-peaked line profiles. A consequence of our single-Gaussian method is that the residual fluxes will be over-estimated for the profiles that differ strongly from a Gaussian shape. Even so, the residual fluxes are modest (Figure 15).

The results of this analysis for all of the spectra of the Bulge planetary nebulae (observed and synthetic) are given in Tables 1 and 2. Both tables present the observed fluxes, observed line widths (FWHM), intrinsic line widths, and, for the deep $H\alpha$ and $[O III]\lambda 5007$ spectra, the residuals with respect to the Gaussian fit. For the shallow $[O III]\lambda 5007$ spectrum and the synthetic extragalactic spectrum,

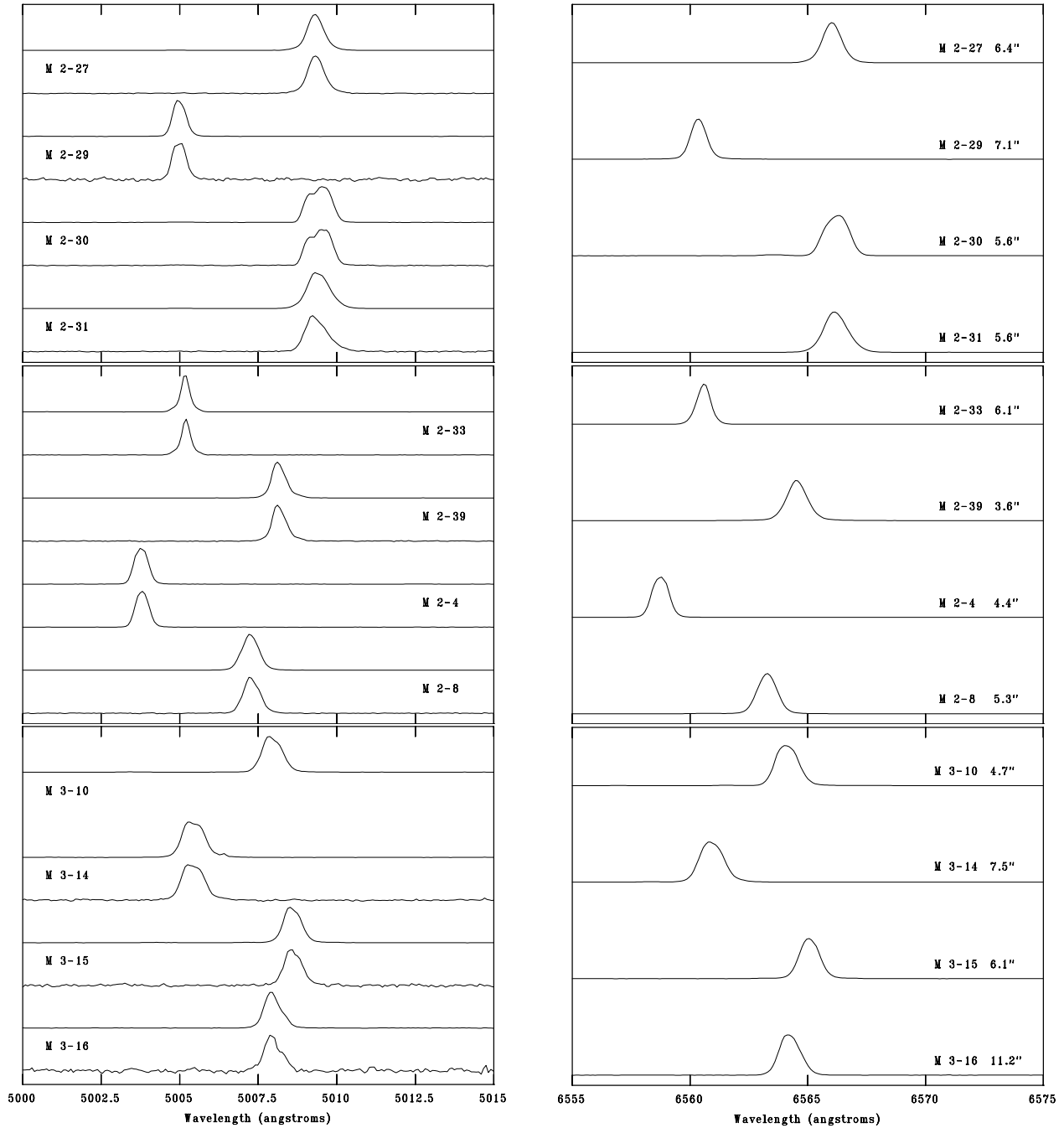


Fig. 7. For M 3-10, only a deep $[\text{O III}]\lambda 5007$ spectrum was obtained. See Figure 2 for further details.

Tables 1–2 present the observed fluxes and line widths (FWHM). With the exception of the residuals with respect to the Gaussian fit, Tables 1 and 2 present the uncertainties in all quantities for each object. All of these uncertainties are the formal uncertainties (one sigma) from INTENS. The results for the extragalactic planetary nebulae will be pre-

sented elsewhere (Richer et al. 2009, in preparation).

In order to derive the intrinsic line widths, the observed line widths must be corrected for several effects that broaden the lines, all of which are assumed to contribute to the observed line width in quadrature. The effects that broaden the true, intrinsic profile are instrumental (σ_{inst}), thermal (σ_{th}),

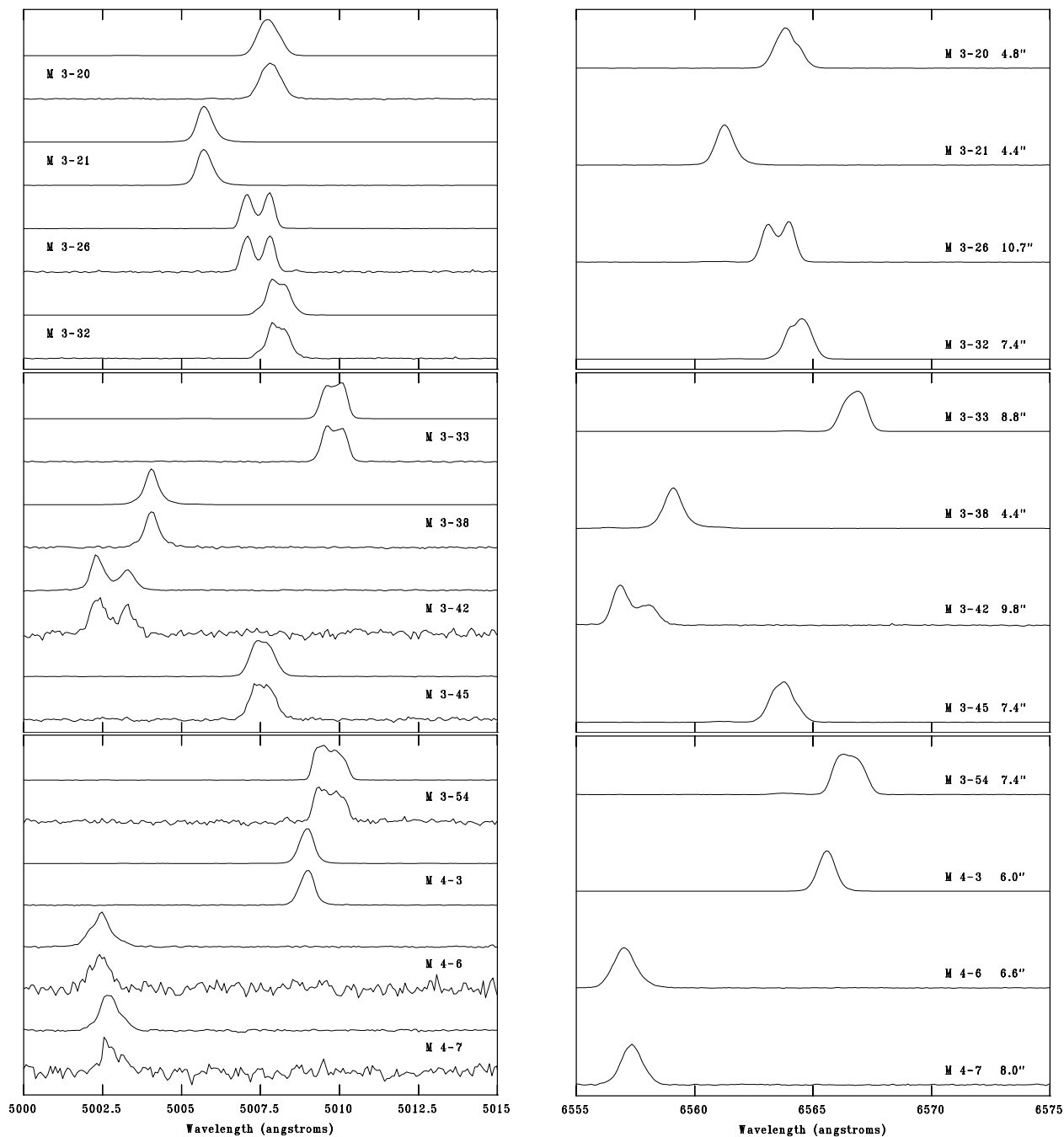


Fig. 8. See Figure 2 for further details.

and fine structure (σ_{fs}) broadening,

$$\sigma_{obs}^2 = \sigma_{true}^2 + \sigma_{inst}^2 + \sigma_{th}^2 + \sigma_{fs}^2. \quad (1)$$

The first term, σ_{true}^2 , is the true, intrinsic line width resulting from the kinematics of the planetary nebula. The instrumental profile has a measured FWHM of 2.5–2.7 pixels, for which we adopted FWHM of 2.6 pixels for all objects (\sim

11 km s $^{-1}$ FWHM). We compute the thermal broadening from the usual formula (Lang 1980, equation 2-243), adopting rest wavelengths of 6562.83 Å and 5006.85 Å for H α and [O III] λ 5007, respectively, the electron temperatures available in the literature (preferentially from the [O III] λ 4363,5007 lines, but from [N II] λ 5755,6584 lines otherwise), and assuming no turbulent velocity. The resulting thermal

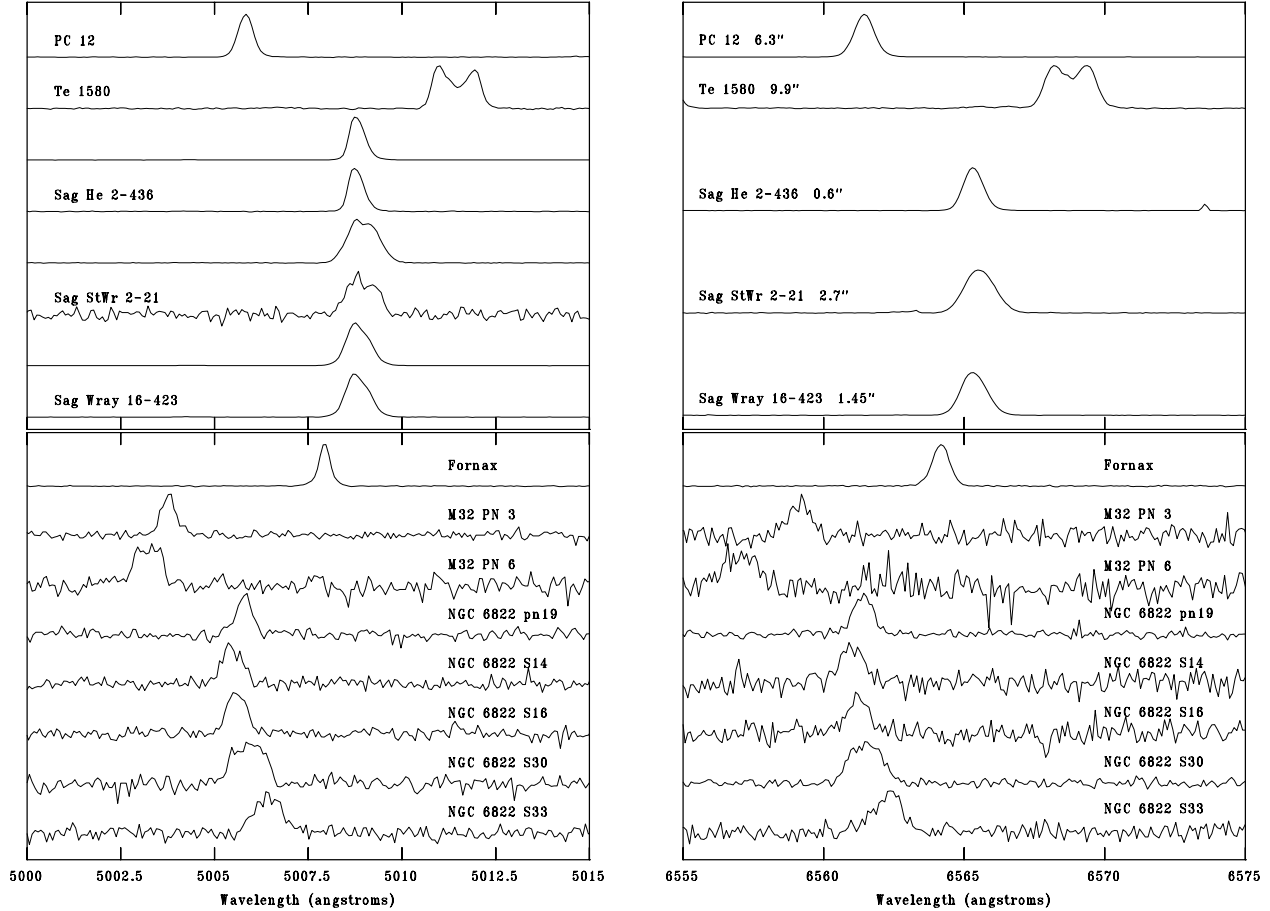


Fig. 9. For the Bulge planetary nebulae Te 1580 and PC 12, only a deep [O III] λ 5007 spectrum was obtained. Deep and shallow spectra were obtained of the three planetary nebulae in the Sagittarius dwarf spheroidal (diameters from Zijlstra et al. 2006). Only deep spectra were obtained for the other extragalactic planetary nebulae. See Figure 2 for further details.

broadening (FWHM) at 10^4 K amounts to 0.47 \AA (21.4 km s^{-1}) and 0.089 \AA (5.3 km s^{-1}) for $H\alpha$ and [O III] λ 5007, respectively. The fine structure broadening, σ_{fs} , was taken to be 3.199 km s^{-1} (FWHM 7.53 km s^{-1}) for $H\alpha$ and zero for [O III] λ 5007 (García-Díaz et al. 2008).

The analysis of line broadening in equation 1 is strictly correct only if all components are Gaussian in shape. Otherwise, a full component deconvolution should be used. Only the thermal and fine structure broadening are truly Gaussian. However, the instrumental profile is only very slightly more square than a Gaussian with the CCD binning used⁵, so treating it as Gaussian should not introduce any significant error, particularly in the case of $H\alpha$ where the thermal and fine structure broadening are more important. The intrinsic line profile for each object, how-

ever, may deviate from a Gaussian shape by amounts that vary depending upon the object's structure and kinematics. The use of equation 1, rather than a full component deconvolution, would be more worrisome were we trying to recover fine details of the line profile or if the lines were intrinsically very narrow. However, the modest S/N of the line profiles of extragalactic planetary nebulae precludes the reliable recovery of detailed line profiles, justifying the simplicity of equation 1.

It is not simple to interpret the resulting FWHM of the intrinsic line width, ΔV , for the Bulge objects (§ 1)

$$\Delta V = 2.3556\sigma_{\text{true}}. \quad (2)$$

The observed intrinsic line width is a luminosity-weighted velocity width for the mass projected within the spectrograph slit, i.e., it represents the spatially-integrated projected outflow velocity of the

⁵Details are available on the observatory website.

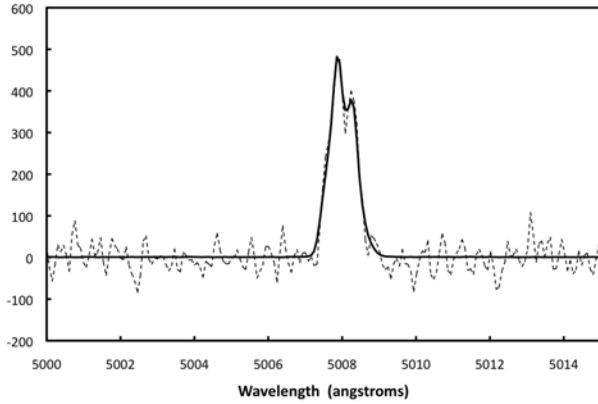


Fig. 10. The synthetic spectra of extragalactic planetary nebulae (dashed line) are constructed using the deep spectra (solid line) of Bulge planetary nebulae. The deep [O III] λ 5007 spectrum is scaled to the typical flux for the spectra of extragalactic planetary nebulae, then a background continuum is added. Here, the deep spectrum of H 1-41 (scaled; solid line) is compared with the synthetic spectrum generated from it. The ordinate is in units of counts.

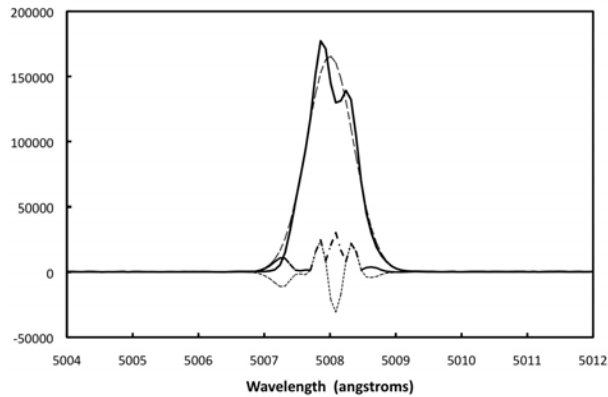


Fig. 11. To compute the residual flux, the Gaussian fit from INTENS (dashed line) is subtracted from the original line profile (solid line). The difference (lower dotted line) is computed and its absolute value (lower dash-dotted line) is determined. The flux contained in the absolute value curve is summed to obtain the residual flux. Here, the residual flux represents 12% of the flux in the Gaussian component. Again, we use H 1-41 as an example. The ordinate is in units of counts.

emitting ions along the line of sight. Note that this velocity is different from the expansion velocity (Schönberner et al. 2005).

The intrinsic line width that we measure should typically exceed the luminosity-weighted line width for the entire object. The spectrograph slit was centered on each Bulge planetary nebula, each of which

is resolved. Therefore, matter near the edges of the objects is excluded from the observations and this matter is likely to have projected velocities similar to the systemic velocity. Consequently, it is likely that our observations miss some matter at the systemic velocity for each object, so the line profile we measure for the matter included within the slit will be slightly larger than the true luminosity-weighted line width. The results presented by Gesicki & Zijlstra (2000) and Rozas et al. (2007) support these arguments. Their simulations of thin, expanding, spherical shells indicate that the line widths we measure may over-estimate the integrated line widths for the entire objects by up to approximately 15%, but that the exact amount will depend upon the fraction of the object covered by the slit and by the real matter and velocity distributions. For the extragalactic planetary nebulae that are not resolved (StWr 2-21 in Sagittarius is the only exception), the line width should be similar to the emission-weighted line width, but the real matter or velocity distributions may also affect this somewhat (Schönberner et al. 2005; Rozas et al. 2007).

Fortunately, we are not concerned with interpreting the line width in what follows. However, since it is clear that this line width will be similar to twice the typical projected outflow velocity, Tables 1 and 2 present half of the line width in velocity units for each object, i.e.,

$$\Delta V_{0.5} = 0.5\Delta V = 1.1778\sigma_{\text{true}}, \quad (3)$$

which we adopt henceforth as our measure of the kinematics of the zone containing the emitting ion (the entire ionized shell in the case of H α).

4. RESULTS

The relation between the line widths in H α and [O III] λ 5007 is shown in Figure 12. Clearly, there is an excellent correlation in almost all cases. The two Bulge planetary nebulae for which the H α line width substantially exceeds the [O III] λ 5007 line width, M 3-42 and K 5-3, are objects with very asymmetric line profiles for which INTENS fit to only one component of the [O III] λ 5007 profile. The narrower thermal width of the [O III] λ 5007 line favors this error. Note that the shallow [O III] λ 5007 spectra have similar intrinsic line widths to those measured in H α . There are also two Bulge planetary nebulae for which the opposite occurs, Cn 1-5 and H 1-59. The first is one of the few objects for which the H α and [O III] λ 5007 spectra were obtained on different nights. The pointings are slightly different, with the

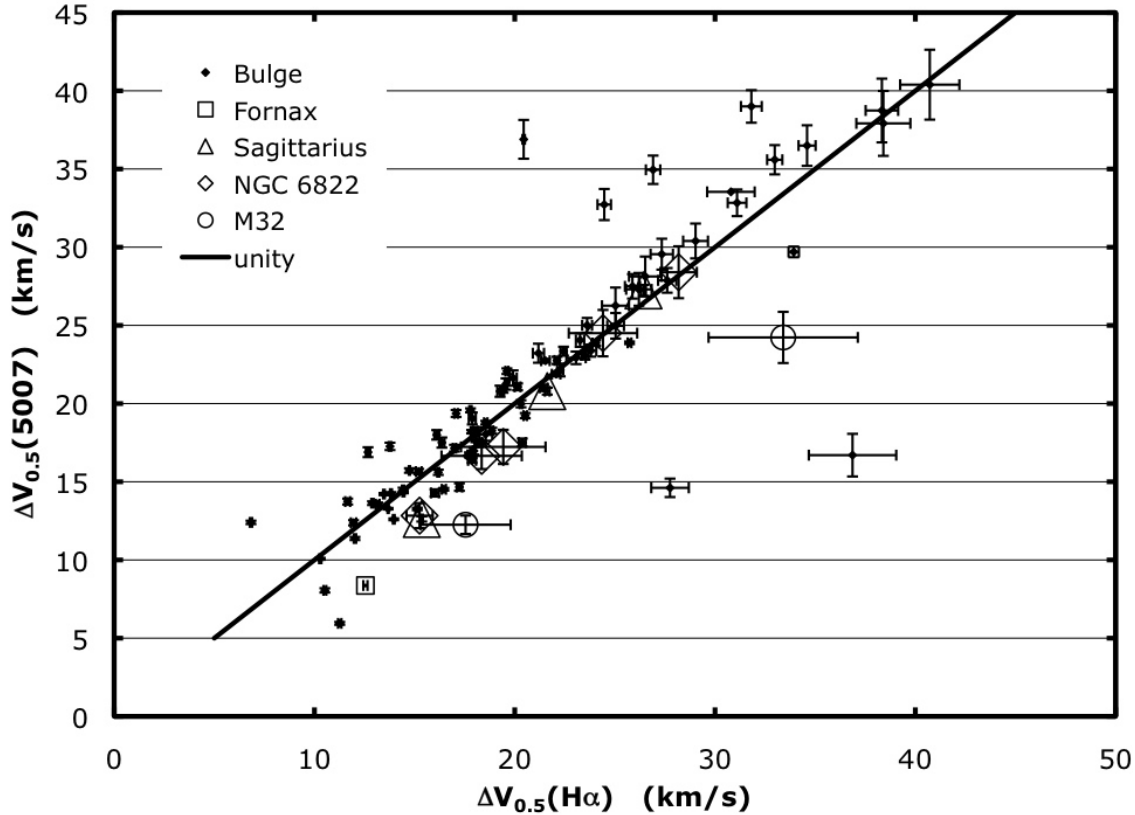


Fig. 12. We find an excellent correlation between the intrinsic $H\alpha$ and $[O\text{ III}]\lambda 5007$ line widths for both Bulge and extragalactic planetary nebulae. The solid line indicates the locus of equal line widths. Therefore, the typical projected outflow velocity deduced from the $[O\text{ III}]\lambda 5007$ line accurately reflects that of the ionized mass in these nebulae. Note that the error bars on the Bulge symbols make these symbols resemble stars when the uncertainties are small.

$[O\text{ III}]\lambda 5007$ observation slightly better centered, so it is possible that the $[O\text{ III}]\lambda 5007$ observation saw considerably more high velocity material. H 1-59 is a very compact object, so if there was some slight flexure between the $H\alpha$ and $[O\text{ III}]\lambda 5007$ observations (the latter was obtained first), the $H\alpha$ observation could have been off-center, which could explain why the $H\alpha$ line width is considerably narrower than the $[O\text{ III}]\lambda 5007$ line width.

The great majority of the Milky Way objects in Figure 12 define a tight relationship. The solid line indicates the locus of identical line widths in $H\alpha$ and $[O\text{ III}]\lambda 5007$. For $H\alpha$ line widths above 20 km s^{-1} , the extragalactic planetary nebulae follow the trend defined by their counterparts in the Bulge. For narrower line widths, the extragalactic planetary nebulae tend to fall on the low side of the Bulge distribution. Whether this is a sampling effect from a small sample or a systematic difference is unclear at present. Overall, however, it appears that the kinematics derived from the $[O\text{ III}]\lambda 5007$ line are very

representative of the kinematics of the entire ionized mass in these objects, whether galactic or extragalactic.

Figures 13 and 14 explore whether the S/N of the observation affects the observed line width. In both figures, the solid line is the locus of identical line widths. In both figures, Cn 1-5 is the lone outlier, for the reasons already discussed. Clearly, within the range of S/N spanned from the deep $[O\text{ III}]\lambda 5007$ spectrum to the shallow and synthetic $[O\text{ III}]\lambda 5007$ spectra, the observed line width is not affected.

Finally, Figure 15 presents the residual flux as a fraction of the flux in the Gaussian component as a function of the line width. There are two fundamental lessons. First, the median fraction of the residual flux is relatively small, 5.5% and 9.5% of the flux in the Gaussian component for the $H\alpha$ and $[O\text{ III}]\lambda 5007$ lines, respectively. Alternatively, the flux represented by the Gaussian component is greater than 75% of the total flux in 94% and 89% of all cases for the $H\alpha$ and $[O\text{ III}]\lambda 5007$ lines, respectively. Second,

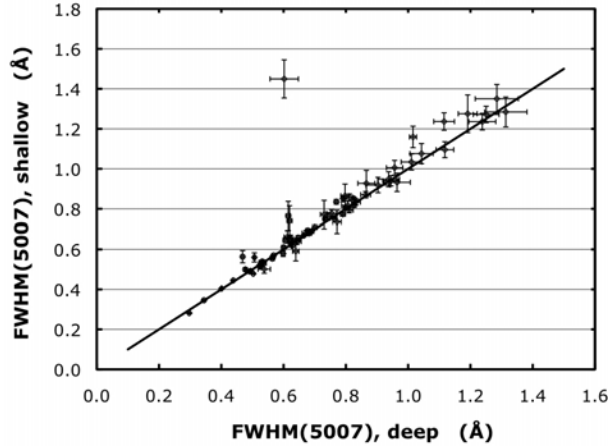


Fig. 13. The observed line widths measured in the shallow and deep $[\text{O III}]\lambda 5007$ spectra are in excellent agreement for our Bulge planetary nebulae. The solid line indicates the locus of identical line widths. This implies that the observed line width is insensitive to the S/N over the range spanned by our deep and shallow spectra.

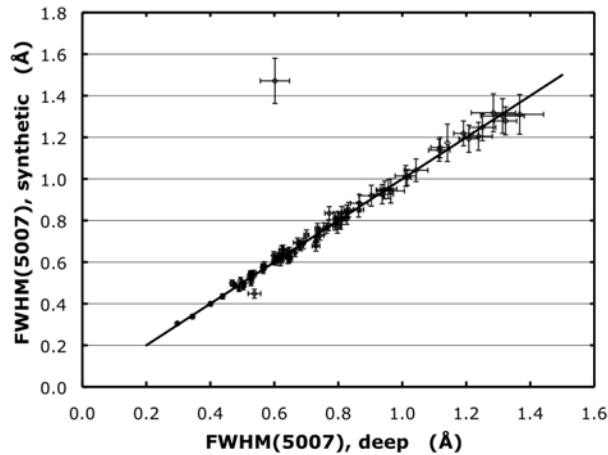


Fig. 14. The observed line widths measured in the deep $[\text{O III}]\lambda 5007$ spectra are in excellent agreement with those measured from the synthetic extragalactic spectra derived from them. Again, the solid line indicates the locus of identical line widths. The median value of the flux ratio between the deep and synthetic spectra is 110. This extends the range in S/N over which the observed line width is insensitive to the total flux to the regime occupied by extragalactic planetary nebulae. Therefore, the line widths measured for extragalactic planetary nebulae should be reliable.

for line widths exceeding about 25 km s^{-1} , the fraction of the residual flux correlates loosely with the line width, for both the $\text{H}\alpha$ and $[\text{O III}]\lambda 5007$ lines.

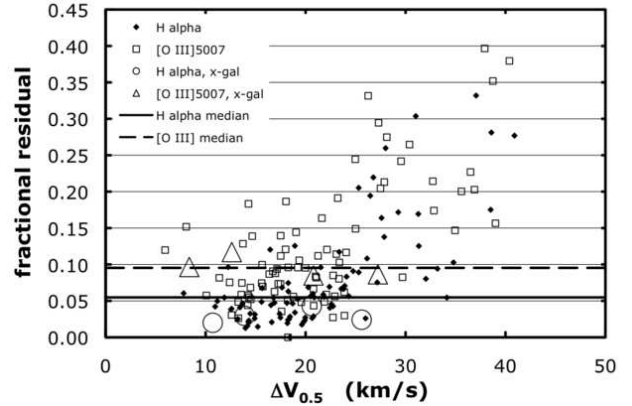


Fig. 15. The fraction of the flux that is not accounted for by the Gaussian component is small. The fraction of residual flux has median values of 5.5% and 9.5% for the $\text{H}\alpha$ and $[\text{O III}]\lambda 5007$ line profiles, respectively. The Gaussian component represents more than 75% of the total flux in 89% and 95% of all cases for the $[\text{O III}]\lambda 5007$ and $\text{H}\alpha$ lines, respectively. Therefore, the Gaussian component adequately describes the kinematics of the majority of the ionized mass in these nebulae.

5. DISCUSSION

Our sample of Bulge planetary nebulae was selected in a way that we hoped would yield a sample of planetary nebulae whose properties were similar to those of bright extragalactic planetary nebulae in environments without star formation. Of particular importance are the criteria of large absolute $\text{H}\beta$ luminosities and large $[\text{O III}]\lambda 5007/\text{H}\beta$ ratios, as are observed in bright extragalactic planetary nebulae in such environments (Richer et al. 2008). For this sample, Richer et al. (2008) found that the more evolved objects (with hotter central stars) have systematically larger sizes and line widths as well as lower $[\text{S II}]$ densities and $\text{H}\beta$ luminosities.

We now consider the issues that motivated this study. How well do the kinematics measured in the $[\text{O III}]\lambda 5007$ line represent the kinematics of the entire ionized shell? How does the limited S/N of observations of extragalactic planetary nebulae affect measurements of the intrinsic line width? Finally, does the limited S/N of observations of extragalactic planetary nebulae significantly limit our understanding of their kinematics?

First, Figure 12 indicates that the $[\text{O III}]\lambda 5007$ and $\text{H}\alpha$ line widths are very similar. The comparison of kinematics in $\text{H}\alpha$ and $[\text{O III}]\lambda 5007$ is telling, since $\text{H}\alpha$ samples all of the ionized mass whereas $[\text{O III}]\lambda 5007$ samples only part of it. Likely, this near equality of the $[\text{O III}]\lambda 5007$ and $\text{H}\alpha$ line widths is a result of our selection criteria. Planetary nebulae

that are luminous in $[\text{O III}]\lambda 5007$ are likely to have O^{2+} zones that occupy a large fraction of the total volume occupied by the ionized mass. It is not so surprising then that the kinematics of the O^{2+} zone are very similar to the kinematics of the entire ionized mass. Therefore, the line width derived from the $[\text{O III}]\lambda 5007$ line for bright extragalactic planetary nebulae should be an accurate reflection of the line width of the entire ionized shell.

In Figure 12, the differences between the galactic and extragalactic planetary nebulae are minimal. Also, though the sample is small, there is no obvious difference between the planetary nebulae in NGC 6822, a star-forming dwarf irregular galaxy, and those in Fornax, Sagittarius, and M32, galaxies that have no current star formation. Since NGC 6822 is currently forming stars, its bright planetary nebulae could conceivably be derived from more massive progenitor stars than those of the planetary nebulae in the other three galaxies (or the bulge of the Milky Way). That the planetary nebulae in NGC 6822 are not anomalous compared to those in the other galaxies would seem to imply that the $[\text{O III}]\lambda 5007$ line widths are equally representative of kinematics of the entire ionized mass for planetary nebulae in all galaxies.

Second, it is clear from Figures 13 and 14 that the line width is not very sensitive to the S/N, at least over the range of S/N probed here. The flux ratio between our deep and synthetic extragalactic spectra has a median value of 110. Therefore, typical observations of extragalactic planetary nebulae should have sufficient S/N for the derived line width to be reliable.

Third, a Gaussian profile, characterized by the measured line width, is an adequate description of the kinematics of the great majority of the ionized mass. The deviations from a Gaussian profile in our deep spectra of planetary nebulae in the Milky Way bulge are small, having median values of 5.5% and 9.5% of the total flux in the lines of $\text{H}\alpha$ and $[\text{O III}]\lambda 5007$, respectively (Figure 15). If we suppose a uniform temperature throughout each object, these fractions also represent the mass fraction whose kinematics deviate significantly from a Gaussian line profile. It is not surprising that the $\text{H}\alpha$ profiles are more nearly Gaussian since their greater thermal width obscures kinematic detail. The extragalactic planetary nebulae in Fornax and Sagittarius do not differ from their Milky Way counterparts regarding the fractional residual flux.

The correlation between the fractional residual flux and the line width is not surprising. How-

ever, both our observational technique or greater kinematic complexity could contribute to the larger residual flux in the objects with larger line widths. Theoretically, we expect the nebular shells to be accelerated while the central star emits a substantial wind (Schönberner et al. 2007; Villaver et al. 2002), an effect that has been found for this sample (Richer et al. 2008) and that is also obvious for the three planetary nebulae in the Sagittarius dwarf spheroidal (Zijlstra et al. 2006). For this sample, there is a loose correlation between line width and diameter, so, even for a fixed geometry, such as a spherical thin shell, the larger objects would be better resolved by our spectrograph slit (fixed width) and would have line profiles that are less Gaussian (e.g., Gesicki & Zijlstra 2000). If, furthermore, the more evolved objects are more spatially inhomogeneous, the deviations from a Gaussian profile will be even more pronounced. Clearly, the fractional residuals we measure for Bulge planetary nebulae should be upper limits to those that would be observed (when feasible) for extragalactic planetary nebulae, i.e., truly spatially unresolved observations should find deviations from a Gaussian profile that are even smaller than those that we observe here.

The foregoing should not be interpreted as indicating that bright planetary nebulae have simple kinematics. H 1-67 is a good example of the contrary (Figure 1). The two-dimensional spectrum clearly presents complex kinematics, but this complexity is not obvious in the spatially-unresolved, one-dimensional spectrum. A Gaussian is a good description of the great majority of the emission (the fractional residual flux is only 17% in $\text{H}\alpha$; Table 2). Nonetheless, the line width describing this Gaussian is not a *complete* description of the kinematics of *all* of the ionized mass, since it does not represent the kinematics of a minority of this mass whose projected motions are more complex.

Very generally, the above results indicate that the observations that will be available for extragalactic planetary nebulae provide reliable information regarding the typical outflow velocity of their ionized mass. Indeed, the direct comparison of the kinematics of Bulge and extragalactic planetary nebulae in Figure 12 is very good. We expect that the line profiles for extragalactic planetary nebulae should be close to Gaussian in shape and that the line width measured from spectra of moderate S/N in the $[\text{O III}]\lambda 5007$ line should accurately reflect the typical projected bulk motion of the great majority of the ionized gas in these objects. It will be difficult to

study fine details of the kinematics, such as jets, of extragalactic planetary nebulae.

Finally, we recall that the issue of the detailed interpretation of the spatially unresolved line profiles remains. This problem is complex and we have not attempted to resolve it here. It will be most profitably attacked once models are developed that include hydrodynamics and photoionization self-consistently and succeed in reproducing the properties of spatially-resolved data, ideally in an ab initio fashion.

6. CONCLUSIONS

We have measured line widths for a large sample of planetary nebulae in the Milky Way bulge in the lines of $H\alpha$ and $[O\ III]\lambda 5007$ using the Manchester Echelle Spectrograph at the 2.1m telescope of the OAN-SPM. The selection criteria for this sample were chosen so as to yield a sample of objects whose properties simulate those of bright extragalactic planetary nebulae in environments without star formation (Richer et al. 2008). We have also obtained similar data for a small sample of the brightest planetary nebulae in the nearby dwarf galaxies Fornax, Sagittarius, M32, and NGC 6822. Our goal is to use our high S/N observations of galactic planetary nebulae to simulate observations of extragalactic planetary nebulae and determine what information can be determined reliably when observing the latter.

Comparing the line widths measured in the $H\alpha$ and $[O\ III]\lambda 5007$ lines, we find very similar values. Therefore, the line width measured for the $[O\ III]\lambda 5007$ line is a good reflection of the typical projected outflow velocity of the entire ionized mass. This result holds for both galactic and extragalactic planetary nebulae. Next, we find that the line widths for our deep spectra are in excellent agreement with those for our shallow or simulated extragalactic spectra for our Bulge planetary nebulae. Therefore, the modest S/N expected for observations of extragalactic planetary nebulae should not be an impediment to studying their kinematics. Finally, we find that departures from a Gaussian shape for the line profiles (deep spectra) of Bulge planetary nebulae are small, typically amounting to 5.5% and 9.5% of the total flux in the $H\alpha$ and $[O\ III]\lambda 5007$ lines, respectively. Alternatively, the Gaussian profile is representative of at least 75% of the emission in 94% and 89% of all cases for the $H\alpha$ and $[O\ III]\lambda 5007$ lines, respectively. So, approximating the line shape as Gaussian is an adequate approximation for most of the flux.

Therefore, the Gaussian line profile and its characteristic width provide an adequate description of

the typical projected outflow velocity of most of the mass of the entire ionized shell. This velocity is neither equivalent to the true nebular expansion velocity (the velocity of the outer shock) nor a complete description of the kinematics of all of the ionized mass. The interpretation of the line profiles in terms of the kinematics of extragalactic planetary nebulae will be very challenging.

Based upon the above results, it is clear that neither the use of the $[O\ III]\lambda 5007$ line nor its likely modest S/N is an impediment to the measurement of the kinematics of the ionized mass in extragalactic planetary nebulae. To the extent that direct comparisons are possible, our results for the bright planetary nebulae in Fornax, Sagittarius, M32, and NGC 6822 do not differ from those for the planetary nebulae in the Milky Way Bulge. We therefore conclude that the line width measured for the $[O\ III]\lambda 5007$ line in bright extragalactic planetary nebulae is an accurate reflection of the typical projected outflow velocity for their entire ionized mass. These results should therefore be a useful reference for the work that will be necessary to enable the detailed interpretation of the kinematics of extragalactic planetary nebulae.

We gratefully acknowledge financial support during this project from Conacyt grants 37214, 43121, and 49447 and from DGAPA-Universidad Nacional Autónoma de México grants 108406-2, 108506-2, 112103, and 116908-3.

REFERENCES

- Aller, L. H., & Keyes, C. D. 1987, *ApJS*, 65, 405
 Arnaboldi, M., et al. 2008, *ApJ*, 674, L17
 Corradi, R. L. M., Steffen, M., Schönberner, D., & Jacob, R. 2007, *A&A*, 474, 529
 Cuisinier, F., Acker, A., & Köppen, J. 1996, *A&A*, 307, 215
 Cuisinier, F., Maciel, W. J., Köppen, J., Acker, A., & Stenholm, B. 2000, *A&A*, 353, 543
 Dopita, M. A., Ford, H. C., Lawrence, C. J., & Webster, B. L. 1985, *ApJ*, 296, 390
 Dopita, M. A., Meatheringham, S. J., Webster, B. L., & Ford, H. C. 1988, *ApJ*, 327, 639
 Escudero, A. V., & Costa, R. D. D. 2001, *A&A*, 380, 300
 Escudero, A. V., Costa, R. D. D., & Maciel, W. J. 2004, *A&A*, 414, 211
 Exter, K. M., Barlow, M. J., & Walton, N. A. 2004, *MNRAS*, 349, 1291
 García-Díaz, Ma. T., Henney, W. J., López, J. A., & Doi, T. 2008, *RevMexAA*, 44, 181
 Gesicki, K., & Zijlstra, A. A. 2000, *A&A*, 358, 1058
 Górny, S. K., Stasińska, G., Escudero, A. V., & Costa, R. D. D. 2004, *A&A*, 427, 231

- Lang, K. R. 1980, *Astrophysical Formulae* (Berlin: Springer)
- Massey, P., Valdes, F., & Barnes, J. 1992, *A User's Guide to Reducing Slit Spectra with IRAF* (Vol. 2B; Tucson: NOAO)
- McCall, M. L., Rybski, P. M., & Shields, G. A. 1985, *ApJS*, 57, 1
- Meaburn, J., Blundell, B., Carling, R., Gregory, D. F., Keir, D., & Wynee, C. G. 1984, *MNRAS*, 210, 463
- Meaburn, J., López, J. A., Gutiérrez, L., Quiroz, F., Murillo, J. M., Valdéz, J., & Pedrayez, M. 2003, *RevMexAA*, 39, 185
- Medina, S., Peña, M., Morisset, C., & Stasińska, G. 2006, *RevMexAA*, 42, 53
- Morisset, C., & Stasińska, G. 2008, *RevMexAA*, 44, 171
- Perinotto, M., Schönberner, D., Steffen, M., & Calonaci, C. 2004, *A&A*, 414, 993
- Ratag, M. A., Pottasch, S. R., Dennefeld, M., & Menzies, J. 1997, *A&AS*, 126, 297
- Richer, M. G., López, J. A., Pereyra, M., Riesgo, H., García-Díaz, M. T., & Báez, S.-H. 2008, *ApJ*, 689, 203
- Rozas, M., Richer, M. G., Steffen, W., García-Segura, G., & López, J. A. 2007, *A&A*, 467, 603
- Sabbadin, F., Turatto, M., Benetti, S., Ragazzoni, R., & Cappellaro, E. 2008, *A&A*, 488, 225
- Santander-García, M., et al. 2008, *A&A*, 485, 117
- Schönberner, D., Jacob, R., & Steffen, M. 2005, *A&A*, 441, 573
- Schönberner, D., Jacob, R., Steffen, M., & Sandin, C. 2007, *A&A*, 473, 467
- Villaver, E., Manchado, A., & García-Segura, G. 2002, *ApJ*, 581, 1204
- Webster, B. L. 1988, *MNRAS*, 230, 377
- Zijlstra, A. A., Gesicki, K., Walsh, J. R., Péquignot, D., van Hoof, P. A. M., & Minniti, D. 2006, *MNRAS*, 369, 875

Sol-Haret Báez: Facultad de Física e Inteligencia Artificial, Universidad Veracruzana, Circuito G. Aguirre Beltrán s/n, Zona Universitaria, Xalapa, Veracruz, México (solharet@hotmail.com).

María Teresa García-Díaz, José Alberto López, Michael G. Richer, and Hortensia Riesgo: Observatorio Astronómico Nacional, Instituto de Astronomía, Universidad Nacional Autónoma de México, Apdo. Postal 877, 22800 Ensenada, B. C., México (tere, jal, richer, hriesgo@astrosen.unam.mx).